Chemosphere 284 (2021) 131254

Contents lists available at ScienceDirect

Chemosphere

journal homepage: www.elsevier.com/locate/chemosphere

Selective graphene-like metal-free 2D nanomaterials and their composites for photocatalysis

Mengdie Yu [a,b], Xingzhong Yuan [a,b], Jiayin Guo [a,b], Ning Tang [a,b], Shujing Ye [a,b], Jie Liang [a,b,*], Longbo Jiang [a,b,**]

[a] College of Environmental Science and Engineering, Hunan University, Changsha, 410082, PR China
[b] Key Laboratory of Environmental Biology and Pollution Control (Hunan University), Ministry of Education, Changsha, 410082, PR China

ARTICLE INFO

Handling EditorY Yeomin Yoon

Keywords:
Graphene
Hexagonal boron nitride
Graphitic carbon nitride
Black phosphorus
Covalent organic frameworks
Photocatalysis

ABSTRACT

From the viewpoint of sustainability, graphene-like metal-free 2D nanomaterials (GMFs) hold great potential in different photocatalytic fields due to their distinct structures and properties. Although their lattice structures are highly similar, the properties of these nanomaterials are in vast diversity owing to the uniqueness of particular atomic arrangement, thus giving rise to their multi-faceted functionalities in photocatalytic process. In this review, we summarize the latest progress of GMFs and their hybrid composites in photocatalytic field, including graphene and its derivatives, hexagonal boron nitride (h-BN), graphitic carbon nitride (g-C_3N_4), black phosphorus (BP) and emerging 2D covalent organic frameworks (COFs). Their unique 2D structure and key photocatalytic properties are firstly briefly introduced. Then a critical discussion on their multiple roles in the activity enhancement of composite photocatalysts is emphasized, which in turn points out the direction of maximizing their functions and guides our efficient construction of hybrid photocatalysts based on above 2D nanomaterials. On this basis, a summary about the hybridization of above 2D metal-free materials is presented, and the merits of 2D/2D hybrid systems are elaborated. Last, we wrap up this review with some summative remarks, covering understanding their own unique strengths and weaknesses by comparison and proposing the major challenges and perspectives in this emerging field.

1. Introduction

With the population explosion and industrialization, the continuous burning of nonrenewable fossil fuels has caused the global aggravation of energy and environmental crisis (Gustavsson et al., 2017). The total global energy consumption is expected to increase from 18.5 TW per year currently to 40.8 TW by 2050, motivating the exploration for alternative sustainable energy technologies (Lewis and Nocera, 2006). Sunlight, an inexhaustible, eco-friendly and easily accessible energy system, has been warranted serious consideration as an ideal power to initiate another pollution abatement and energy utilization (Jiang et al., 2017a). Particularly, photocatalysis, capable of directly capturing and harnessing solar energy into chemical energy, represents a safe, cost-effective and prospective technology (Che et al., 2020; Orooji et al., 2020; Wu et al., 2020). The development of highly active and diversified photocatalysts is a critical determinant of photocatalysis. Since Fujishima and Hondafrom first demonstrated experimentally water splitting over titanium dioxide (TiO_2) electrode under light irradiation in early 1970s (Finegold and Cude, 1972), miscellaneous photocatalyst materials, such as metal oxides (ZnO (Serrà et al., 2020), WO_3 (Meng et al., 2021), Fe_2O_3 (Wu et al., 2020), etc.), certain metal sulphides (CdS Zhou et al., 2020), ZnS (J. Zhou et al., 2020), MoS_2 (Singh et al., 2020), etc.) and metal nitrides (Ta_3N_5 (Li et al., 2020), etc.) have been extensively studied. Though metal-based photocatalysts have been in ever-growing demand, they still suffer from obvious drawbacks like high cost, corrosion susceptibility and toxicity (Wu et al., 2018). In "green" 21st century, metal-free photocatalysts, due to their earth abundance, good durability in acidic/basic media and environmental friendliness, are rapidly but steadily emerging in parallel to metal-based systems (Hu et al., 2019).

In the family of metal-free photocatalysts, two-dimensional (2D) nanomaterials possess astonishing physicochemical properties dictated by their sheet-like structures with the atomic-scale thickness, which are inherently superior to their traditional 3D counterparts (Zhao et al., 2020). The merits of a two-dimensional structure for photocatalysis

* Corresponding author. College of Environmental Science and Engineering, Hunan University, Changsha, 410082, PR China.
** Corresponding author. College of Environmental Science and Engineering, Hunan University, Changsha, 410082, PR China.
E-mail addresses: liangjie@hnu.edu.cn, liangjie82@163.com (J. Liang), jianglongbo@hnu.edu.cn (L. Jiang).

https://doi.org/10.1016/j.chemosphere.2021.131254
Received 11 April 2021; Received in revised form 14 June 2021; Accepted 15 June 2021
Available online 18 June 2021

Nomenclature

GMFs	Graphene-like metal-free 2D nanomaterials
GR	Graphene
GO	Graphene oxide
rGO	Reduced graphene oxide
h-BN	Hexagonal boron nitride
g-C_3N_4	Graphitic carbon nitride
BP	Black phosphorus
COFs	Covalent organic frameworks
MOFs	Metal-organic frameworks
2D	Two-dimensional
3D	Three-dimensional
QDs	Quantum dots
CB	Conduction band
VB	Valence band
DFT	Density functional theory
PTE	Photothermal effect
TC	Tetracycline
RhB	Rhodamine B
MB	Methylene blue
MO	Methyl orange
CR	Congo Red
FT-IR	Fourier-transform infrared spectroscopy
TEM	Transmission electron microscopy
SEM	Scanning electron microscopy
EIS	Electrochemical impedance spectroscopy
NIR	Near infrared radiation
UV	Ultraviolet
PL	Photoluminescence
TEOA	Triethanolamine
ALD	Atomic layer deposition
CVD	Chemical vapor deposition
MC	Monte Carlo
MD	Molecular dynamics
SPV	Surface photovoltage

relates to following aspects: (i) the high lateral-area-to-thickness ratio, resulting in abundant exposure of surface active sites to take part in the photocatalytic reaction (Sun et al., 2015); (ii) the short pathways for charge-carrier transport towards surface for photoredox reaction, leading to lower electron-hole pair recombination rate compared with traditional 3D photocatalysts (Niu et al., 2012; She et al., 2016); (iii) the tunable number of layers, allowing band gap and electronic states modulation (Dong et al., 2015; Kouser et al., 2015); (iv) rich surface defects, improving conductivity and facilitating charge transfer to adsorbates (Zhao et al., 2020); (v) excellent mechanical properties, offering high durability and stability typically in the case of combination with other materials (Yang et al., 2016). Irrefutably, the above advantages can impart metal-free 2D nanomaterials with remarkable activities when they are synergistically exploited and optimized. The discovery of more efficient metal-free 2D nanomaterials is an urgent priority for practical photocatalysis technology.

The triumphant fabrication of graphene via mechanical exfoliation from a mass of graphite in 2004 triggered ripples of excitement in the bound of science and technology (Novoselov et al., 2004). Since then, graphene has been prospering in the photocatalysis field by reason of its astonishing chemical, electrical and mechanical properties (Balandin et al., 2008; Lee et al., 2008; Nair R. R. et al., 2008). Quite an accomplishment of graphene throws new light on searching for other graphene-like metal-free 2D nanomaterials (GMFs) but with characteristics that graphene lacks. Meanwhile, their similar lattice structure endorses a promising platform to design new nanostructures or nanocomposites, that is, more versatility in structure and function can be obtained through using individual GMFs as basic components (Novoselov et al., 2016). Based on graphite carbon nitride (g-C_3N_4), one of representatives of GMFs, our research group have constructed several high-efficiency photocatalysts for the removal of pollutants in the environment recently, including metal-free sulfur and phosphorus co-doped g-C_3N_4 (Jiang et al., 2017b), metal-free nitrogen self-doped g-C_3N_4 (Jiang et al., 2019), a metal-free hexagonal boron nitride (h-BN) nanosheet/g-C_3N_4 heterojunction photocatalyst (Jiang et al., 2018d), a phosphorus-doped g-C_3N_4/g-C_3N_4 (PCN/CN) isotype heterojunction composite photocatalyst (Jiang et al., 2018c) and a direct double Z-scheme WO_3/g-C_3N_4/Bi_2O_3 photocatalyst (Jiang et al., 2018a). Besides, hexagonal boron nitride (h-BN), black phosphorus (BP) and emerging 2D covalent organic frameworks (COFs) have also been widely utilized in photocatalytic energy and environmental applications (Li et al., 2019; Yang et al., 2020).

Although the lattice structures of graphene-like metal-free 2D nanomaterials are highly similar, their properties are in vast diversity owing to the uniqueness of specific atomic arrangement, thus giving rise to their multi-faceted functionalities in photocatalytic process (Liu and Zhou, 2019). In the prior literature, some excellent reviews centered on the realms of synthesis methods, properties, related applications (e.g., CO_2 reduction, H_2 evolution, organic contaminants degradation), and modification routes (e.g., doping, copolymerization, heterojunction construction) to tune the active sites and electronic states of single material (Chen et al., 2018; Guo et al., 2021b; Rahman et al., 2020; Yu et al., 2018). Nevertheless, these reviews didn't completely lay stress on the photocatalytic mechanism of composite materials, let alone the functions of each constituent material for photocatalytic activity enhancement. In addition, comprehensive reviews focused on contrasts and critical comments on a series of graphene-like metal-free 2D photocatalysts are rarely reported. Therefore, a systematically comparative overview of the various graphene-like metal-free 2D photocatalysts is necessary to highlight their respective characteristics and differences as well as disclose the origin of the activity enhancement in composites. In this review, we address the recent progress of GMFs and their hybrid composites in photocatalytic field, including graphene and its derivatives (Chapter 2), hexagonal boron nitride (h-BN) (Chapter 3), graphitic carbon nitride (g-C_3N_4) (Chapter 4), black phosphorus (BP) (Chapter 5) and emerging 2D covalent organic frameworks (COFs) (Chapter 6). In each chapter, we first briefly introduce their unique 2D structure and key photocatalysis-related properties and then critically elaborate their multiple roles in the activity enhancement of composite photocatalysts. Later, the composite systems based on above 2D metal-free materials are also studied (Chapter 7). Meanwhile, the merits of 2D/2D hybridization are proposed. Finally, this review concludes with some thoughts about the major challenges and perspectives in this emerging field.

2. Graphene, GO, rGO: only efficient electron transfer?

The discovery of graphene dates back to 2004 when Novoselov et al. prepared 2D single-atom-thick films by repeated mechanical exfoliation, which triggered a revolution in science and technology (Novoselov et al., 2004). Although there are diverse methods to synthesize graphene, each of them has pros and cons taking the applicability, cost, yield and quality of as-obtained samples into account. Relatively reasonable selection of method according to the intended use can reduce cost and improve practicability. For instance, solution-based techniques tend to be adopted to construct graphene-based composites. Composed of sp^2-hybridized carbon atoms that are tightly wrapped into an alveolate lattice, graphene with zero band gap possesses many exceptional

physical and chemical properties, including high mechanical strength (tensile strength: 130.5 GPa, Young's modulus: 1 TPa) (Lee et al., 2008), extremely massive specific surface area (2630 $m^2\ g^{-1}$) (Stoller et al., 2008), high thermal conductivity (3000–5000 W $m^{-1}\ K^{-1}$) (Loh et al., 2010), marvellous intrinsic charge carriers mobility (at room temperature: 200,000 $cm^2\ V^{-1}\ s^{-1}$) (Balandin et al., 2008), plus its high optical transmittance (97.7%) (Nair et al., 2008). In recent years, graphene-derivative materials, like graphene oxide (GO), reduced graphene oxide (rGO), have displayed much more appealing characteristics. Different from the hydrophobic properties of graphene, the oxygen-containing functional groups (e.g., –OH, =O, –COOH and –C═O) on the panel and edge of GO, endue it with the ability to disperse easily in aqueous solutions and to interact efficiently with other various compounds (Yeh et al., 2013). Moreover, the conversion of graphene towards a semiconductor with a certain bandgap come true due to the broken sp^2 conjugated network structure in GO and the restrictions of the π-electrons in the isolated sp^2 domains (Boukhvalov and Katsnelson, 2008; Loh et al., 2010). GO has the potential to be a candidate for outstanding non-metal photocatalysts because its band structure is linked with its oxidation degree and can be adjusted by selecting proper synthetic methods (Yeh et al., 2010). Reduced graphene oxide (rGO) are produced by upon reduction of GO. Its oxygenation levels are different from GO in despite of containing oxygen functional groups and its intrinsic structural and electronic characteristics can be recovered in part compared with graphene (Yang et al., 2014). With oxygen functionalities, GO and rGO can interact with comprehensive precursors and structures through non-covalent bonding (Π-Π stacking, hydrophobic interaction and electrostatic interaction), covalent bonding (cycloaddition, condensation, and polymerization reactions) (Jilani et al., 2018). These advantageous properties promote graphene and its derivatives enormous potentials for various applications, the most promising directions of which is to construct heterogeneous graphene-based composite photocatalysts (Yang et al., 2014; Zhang and Xu, 2016). Thanks to its favorable electronically conductive 2D structure, the most-acknowledged role of graphene is demonstrated as a sink for accepting, transporting, and shuttling electrons generated from the photoexcitation of photoactive sites in the composite photocatalysts (Karim et al., 2020; Mahmoudi et al., 2019). In the graphene-based photocatalysts, the common form of graphene is, in fact, graphene-derivative materials (GO, rGO) with complex and various optical and electronic properties instead of the ideal and well-defined 2D one-atom-thick carbon sheet (Zhang et al., 2015). To this degree, are the roles of graphene only efficient electron transfer? Hence it is certainly worth to give a critical summary about the key roles of graphene played in the graphene-based composite photocatalysts.

2.1. Photoelectron transfer mediator and acceptor

In virtue of the low Fermi level of graphene (−0.08 V *vs.* NHE), the E_{CB} of most semiconductors is more negative than it (Gao et al., 2011; Jin et al., 2010). Once they come to contact with each other, the photo-induced electrons will automatically transfer from the conduction band of semiconductors to 2D graphene nanomaterials. Besides, the high charge carriers mobility (200,000 $cm^2\ V^{-1}\ s^{-1}$) of graphene guarantees it that electrons transfer in the network of graphene with freedom. On the basis of these two aspects, graphene is a good electron mediator and acceptor to cut down recombination of the electron–hole pairs, thus improving the photocatalytic activity of composite photocatalysts. For example, Yuan et al. grew SnS_2 quantum dots (QDs) on rGO for better visible-light-activated photocatalytic reduction of Cr(VI) (Yuan et al., 2017). Compared with the redox potential of graphene ($E(G/G^{\cdot-})$ = −0.08 V *vs.* NHE), the more negative CB of SnS_2 (E_{CB} = −0.91 V *vs.* NHE) provides enough actuating force for the transfer of photoinduced electrons from CB of SnS_2 to graphene, and then the Cr(VI)-to-Cr(III) conversion is easy to come true on the surface of graphene. With the introduction of rGO, the exposure of more active sites, the reduction of carrier recombination and the acceleration of surface electron transfer can be observed in the photocatalytic results.

Besides as the electron sink and electron acceptor, graphene can also act as electron transfer mediator between the photocatalyst and the cocatalyst. Lang et al. served graphene as the conductive "bridge" between plasmonic Ag(100) nanocubes and TiO_2(001) nanosheets for photocatalytic H_2 evolution (Lang et al., 2018). It's known that the Schottky junction can be established between the semiconductor and metal only under the condition that the work function of semiconductor (W_s) is smaller than that of metal (W_m) ($W_s < W_m$) (Jiang et al., 2016). As shown in Fig. 1a, without the introduction of rGO, no Schottky barrier occurred between the metal Ag (W_m = 4.28 eV) and the semiconductor TiO_2 (W_s = 4.89 eV), leading to the injected hot electrons flowing back to metal and then recombining with hot holes. While in the Ag(100)-rGO-TiO_2(001) structure (Fig. 1b), rGO nanosheets played the role of the conductive channel which can efficiently promote the hot electron streaming from plasmonic Ag to TiO_2 nanosheets, breaking the restriction and achieving the transfer of hot electrons from the metal Ag with smaller work function to the semiconductor TiO_2 with larger work function.

2.2. Enhancing adsorptivity for reactants

As a prerequisite for photocatalytic reaction, surface adsorption could promote the photocatalytic process, while the subsequent decomposition of as-adsorbed reactants by photodegradation could occur, thus regenerating the active sites for the removal of pollutants circularly (Zhang et al., 2011). Many different kinds of functional groups such as amino, carbonyl, epoxy, and hydroxyl groups and defect sites on the large specific surface of 2D rGO/GO materials donate graphene another fundamental and significant role of enhancing the adsorption capacity in graphene-based composites as shown in Fig. 2a (Upadhyay et al., 2014). Moreover, depending on the different target reactants i.e., ionic pollutants, gas molecules, dyes, and aromatic compounds, the adsorption interaction types of which on graphene-based composites have some differences, including electrostatic attraction, chemical interaction, or physical adsorption. For example, the different mechanism of dye molecules (CR, MB) adsorption by GO was illustrated by Natarajan and Bajaj in Fig. 2b, c (Natarajan and Bajaj, 2016).

Generally, the appearance of π-π stacking between organic pollutants and the aromatic regions of graphene which contain aromatic rings facilitates the adsorption of reaction substrates onto the surface of photocatalyst thereby enhancing the photoredox activity (Lee et al., 2012). As a representative example, Si and coworkers believed that graphene with the large and smooth graphite layer could produce π-π interaction and had good affinity to dye molecules, thus easily adsorbing MB with π electrons by the π-π bonds as well as hydrogen bonds, which increased the exposure of photocatalyst to pollutants and realized the enhanced photocatalytic degradation performance of rGO/$BiFeO_3$ particles for MB removal (Si et al., 2018).

Differences in synergistic adsorption-photocatalytic behavior between GO-based and rGO-based composites photocatalysts have been reported a lot. Through one-pot co-precipitation method, Hu et al. designed $Bi_2Fe_4O_9$/GO and $Bi_2Fe_4O_9$/rGO at a low temperature of 95 °C where mass ratio of GO to $Bi_2Fe_4O_9$ was 4.5 wt% and evaluated their hydrophobic BPA synergistic adsorption-photocatalytic degradation respectively (Hu et al., 2015). According to the adsorption isotherms in Fig. 3a, the adsorption capacity of $Bi_2Fe_4O_9$/GO4.5 was inferior to $Bi_2Fe_4O_9$/rGO4.5, which could be ascribed to the restricted π-π stacking interaction by excessive functional groups (–O–, –OH, and –COOH) of GO. As for $Bi_2Fe_4O_9$/rGO4.5 composites, π-π stacking interaction which was formed between benzene ring in BPA and the skeletal structure of rGO enhanced the adsorption of BPA (Fig. 3b). In another study, Adamu et al. converted GO into rGO via the thermal reduction at around 250 °C, which donated as TGO. Then TiO_2-GO and TiO_2-TGO composites were both synthetized for the photocatalytic phenol removal (Adamu et al.,

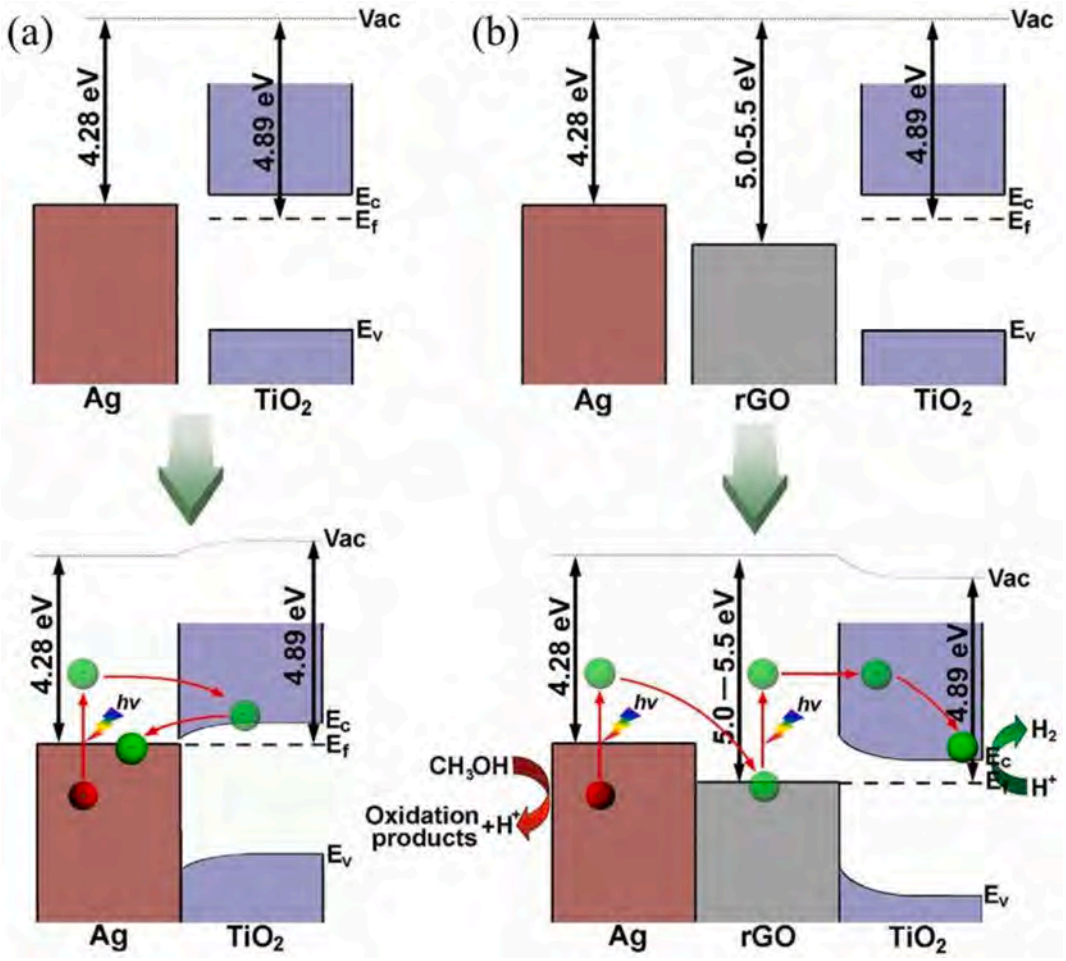

Fig. 1. Schematic representation of the photocatalytic mechanism for the (a) Ag–TiO_2 and (b) Ag-rGO-TiO_2 samples under visible light irradiation. Reprinted with permission from Ref (Lang et al., 2018). Copyright 2018, Elsevier.

2016). After 0.25 wt% GO or TGO was integrated within the TiO_2 matrix, photocatalytic activity reached the highest as the adsorption of phenol enhanced. TiO_2-TGO with 2D structure consisting of π-conjugation could adsorb pollutes by π-π interaction and hydrogen bonds while TiO_2-GO with more defect abundance and poor delocalization of electrons could adsorb pollutants only by hydrogen bonds, thereby the latter (Fig. 3c) had worse adsorptivity than the former (Fig. 3d). Ratios of graphene in composites photocatalysts have an effect on the adsorptivity (Zhang et al., 2010). Ranjith's group fabricated different nanocomposites (ZnO NR-rGO) with a series of rGO addition ratios. As the content of rGO in the ZnO NR-rGO nanocomposites increased, the adsorption of rhodamine B (RhB), methylene blue (MB) and methyl orange (MO) increased correspondingly (Fig. 3e) (Ranjith et al., 2017). However, excessive rGO would act as electron-hole recombination center and prevent the light diffusion of ZnO, thus impressing negatively on photocatalytic efficiency, which was called as shield effect. As can be seen from Fig. 3f, while the ratio of rGO increased over 7.5 wt%, the photocatalytic efficiency began depressing in the GZ12.5 and GZ10.0.

2.3. Enhancing optical absorption range and intensity

Photocatalysis, initiated by photoexcitation, depends on light absorption unquestionably. Wide band gap semiconductors such as ZnO and TiO_2, occupying a lot in photocatalysts under investigation, cannot be driven under visible light which hinder their wide practical applications (Addamo et al., 2006). Combining with graphene has been proved to be capable of extending the light response of semiconductors from ultraviolet to visible light region. One possible underlying mechanism of that can be described as the following: the formation of chemical bonding (M−C or M–O–C, M represents metal) at the interface between graphene and semiconductors by appropriate reaction pathways produces new energy levels within the electronic structure of semiconductors, thus narrowing its band gap and increasing the visible-light response (Chen et al., 2013).

For example, Ti–O–C bonding produced because the unpaired π electrons on GO could chemically interact with Ti atoms on TiO_2, which narrowed the bandgap of TiO_2 and extend its light absorption range (Fig. 4a) (Lee et al., 2012; Yeh et al., 2013). In view of that, Chen et al. reported a series of hydrothermally prepared TiO_2-rGO nanocomposites under different temperature conditions and discussed about the effect of Ti–O–C chemical bonds between graphene and TiO_2 interfaces to photocatalytic performance (Chen et al., 2018). The Ti–O–C bonding usually vibrates at 798 cm^{-1}; its formation could be confirmed by the minor fluctuations approximately 800 cm^{-1} of TiO_2-rGO series in the FT-IR spectra. Compared to TiO_2 P25 itself, much more improved photo-responses of visible light and obviously narrowed band gaps (from 3.0 eV to 2.5 eV) of all TiO_2-rGO series samples could be observed. Moreover, in this study, the higher hydrothermal temperature leads to the narrower band gap and the more enhanced photocatalytic activities.

2.4. Photosensitizer

As discussed above, the addition of graphene may narrow the band gap of semiconductor due to the appearance of chemical bonds at the

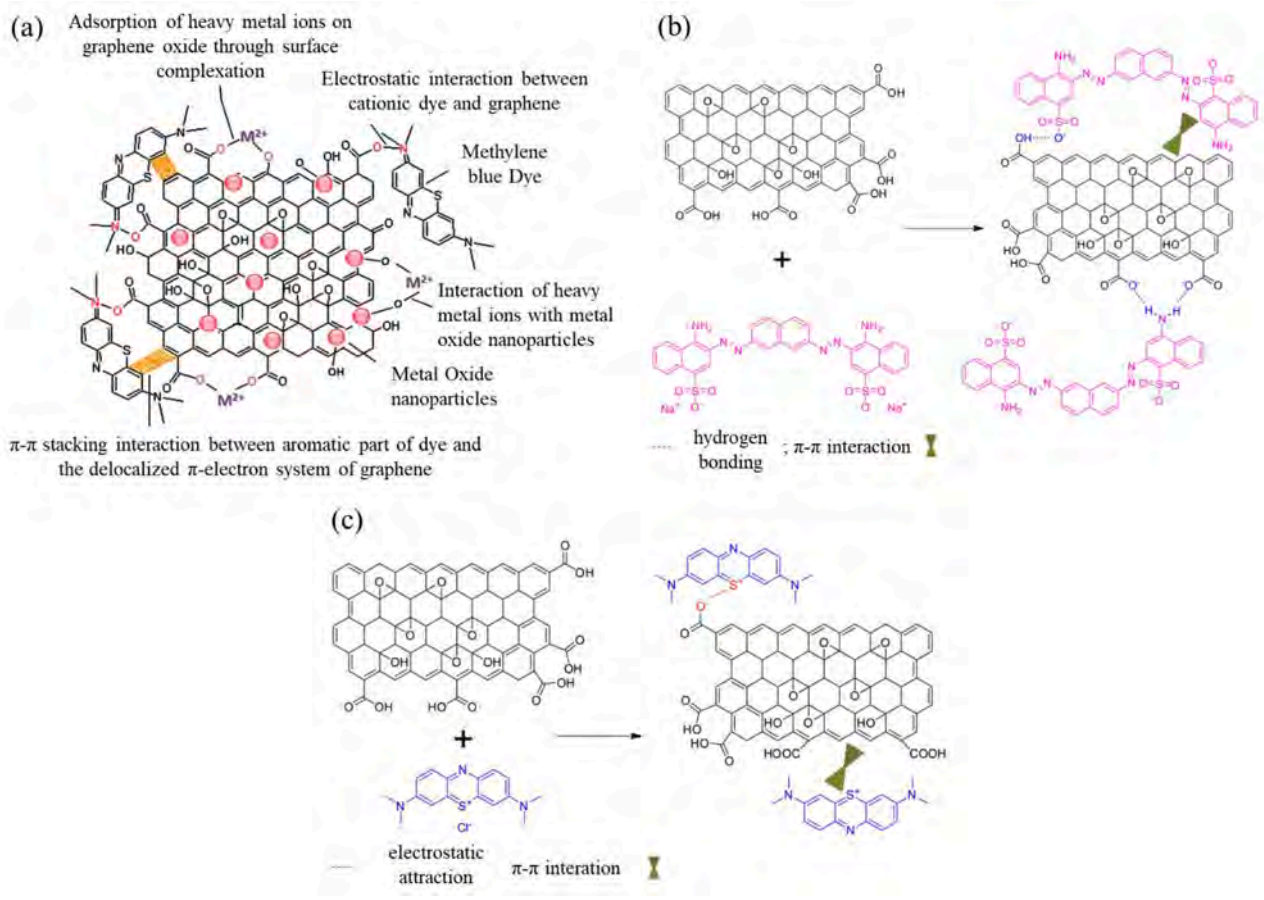

Fig. 2. (a) Different modes of interactions in the adsorption of pollutants on metal oxide/graphene oxide. Reprinted with permission from Ref (Upadhyay et al., 2014). Copyright 2014, The Royal Society of Chemistry. (b) Schematic illustration of the mechanism of congo red (CR) adsorption by GO. (c) Schematic illustration of the mechanism of methylene blue (MB) adsorption by GO. Reprinted with permission from Ref (Natarajan and Bajaj, 2016). Copyright 2016, Elsevier. (For interpretation of the references to colour in this figure legend, the reader is referred to the Web version of this article.)

interface between semiconductors and graphene, resulting in the expansion of the optical absorption range. Interestingly, it was also observed that the photoexcited valence electrons could be directly injected from graphene to the CB of semiconductor under visible-light irradiation followed by participating in the reduction reaction on the surface of semiconductor, thus broadening visible-light response without narrowing the band gap. And this new role of graphene was called "photosensitizer".

As early as 2011, the role of GO as photosensitizer was theoretically evidenced. Du et al. first studied the interfacial interactions in hybrid graphene/rutile TiO_2(110) nanocomposite via large-scale density functional calculations. They proposed that the photoinduced electrons could be directly excited from the upper VB of graphene to the CB of titania under visible light irradiation, which was in line with the wavelength dependence measurement of the photocurrent response (Du et al., 2011). Then they researched the graphene/g-C_3N_4 interfacial charge transfer using hybrid functional DFT calculations. A top view of the charge density difference plots at the graphene/g-C_3N_4 interface was shown in Fig. 4b. The formation of a big electron−hole puddle led to the redistribution of charge density. There was so strong an electron coupling inducing a new optical transition that the interlayer charge in the VB of graphene was also directly excited to the CB of g-C_3N_4. After the coupling, a 70 meV-gap-opening was achieved in graphene, which suggested that g-C_3N_4 offered a suitable substrate for graphene (Du et al., 2012). Unfortunately, above studies couldn't prove amply the role of graphene as photosensitizer.

Furthermore, experimentally, the robust and direct evidence on revealing the function of graphene as photosensitizer for semiconductors during an actual photocatalytic process was available in Xu's study. The ZnS-rGO nanocomposites featuring intimate interfacial contact for selective oxidation of alkenes and alcohols exhibited visible light photoactivity. The structure-photoactivity correlation and photocatalytic mechanism study adopting a string of radical scavengers disclosed that graphene in the ZnS-rGO nanocomposites acted as a macromolecular organic dye-like photosensitizer. Graphene could be photoexcited from ground state GR to excited state GR* upon visible light irradiation and then photogenerated electrons transferred to the CB of ZnS (Zhang et al., 2012). Subsequently, they found the same photosensitizer role of graphene on rGO-ZnO composites toward photodegradation of Cr(VI) under the visible-light condition (Yang and Xu, 2013). Moreover, they recommended three basic principles for exploring the exact photosensitizer role of graphene in visible-light-driven graphene-semiconductor composite photocatalysts by summing up their own research experience and contrasting some other studies. (i) It should not occur that the semiconductor in the graphene-semiconductor composites can be band gap-photoexcited under visible light irradiation (Kiran et al., 2009). (ii) It is crucial to guarantee the intimate and specific interfacial interaction between graphene and the semiconductor (Yang and Xu, 2013). (iii) It should be considered rigorously to circumvent the self-induced photosensitization effect (e.g., organic dye photosensitization for semiconductor) by choosing suitable probe reactions (Bai et al., 2012). Very recently, Chen et al. successfully fabricated monodisperse ZnS-coated rGO nanocomposites by a facile hydrothermal treatment for photocatalytic methylene blue (MB) degradation (Chen et al., 2019). They concluded that the enhanced visible photocatalytic activity could be ascribed to the

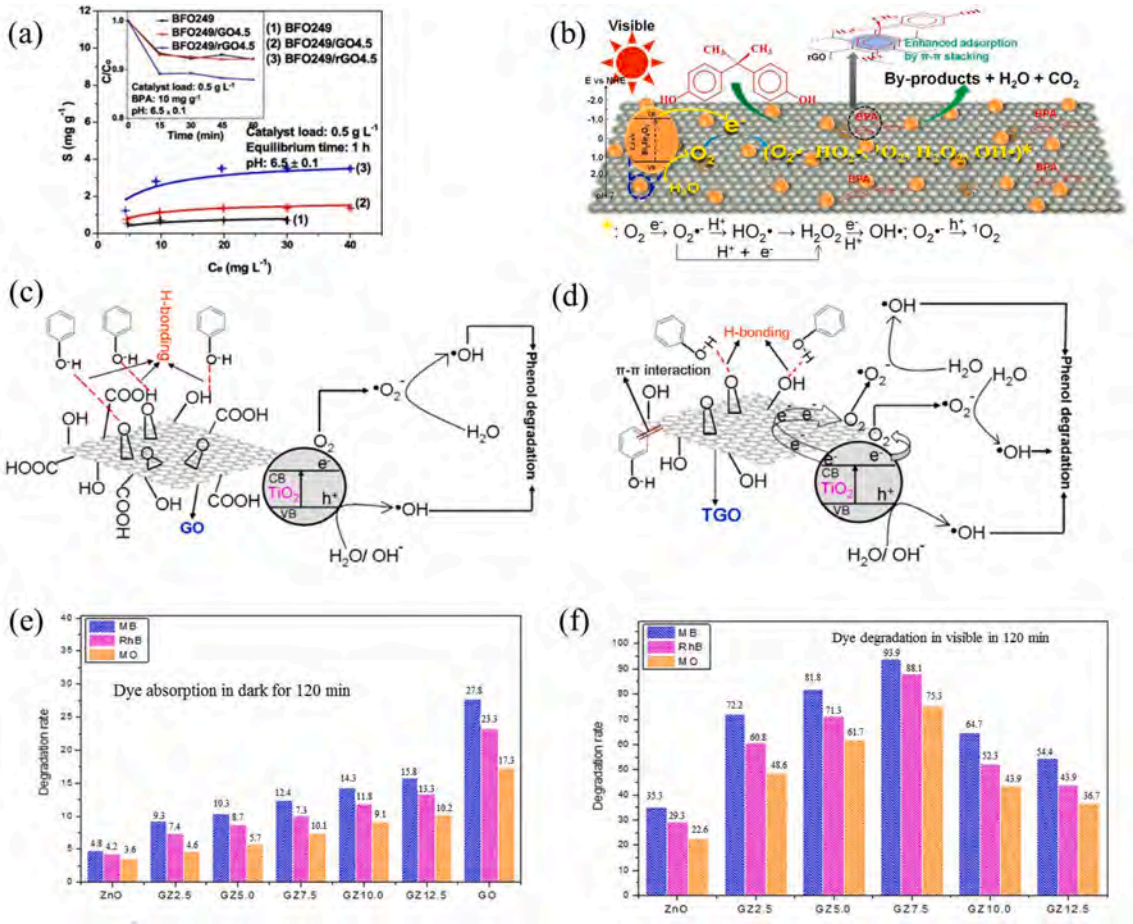

Fig. 3. (a) Adsorption isotherms and time-dependent adsorption (inset) of BPA for BFO249, BFO249/GO4.5 and BFO249/rGO4.5. (b) Schematic illustration of proposed photocatalytic mechanism of BFO249/rGO4.5. Reprinted with permission from Ref (Hu et al., 2015). Copyright 2015, Elsevier. Proposed mechanisms of phenol degradation in oxygen by (c) TiO_2-0.25% GO and (d) TiO_2-0.25% TGO composites. Reprinted with permission from Ref (Adamu et al., 2016). Copyright 2016, Elsevier. Adsorption (e) and comparative photocatalytic degradation (f) of different dye pollutants for the pure ZnO NR and ZnO NR-rGO nanocomposite. Reprinted with permission from Ref (Ranjith et al., 2017). Copyright 2017, Elsevier.

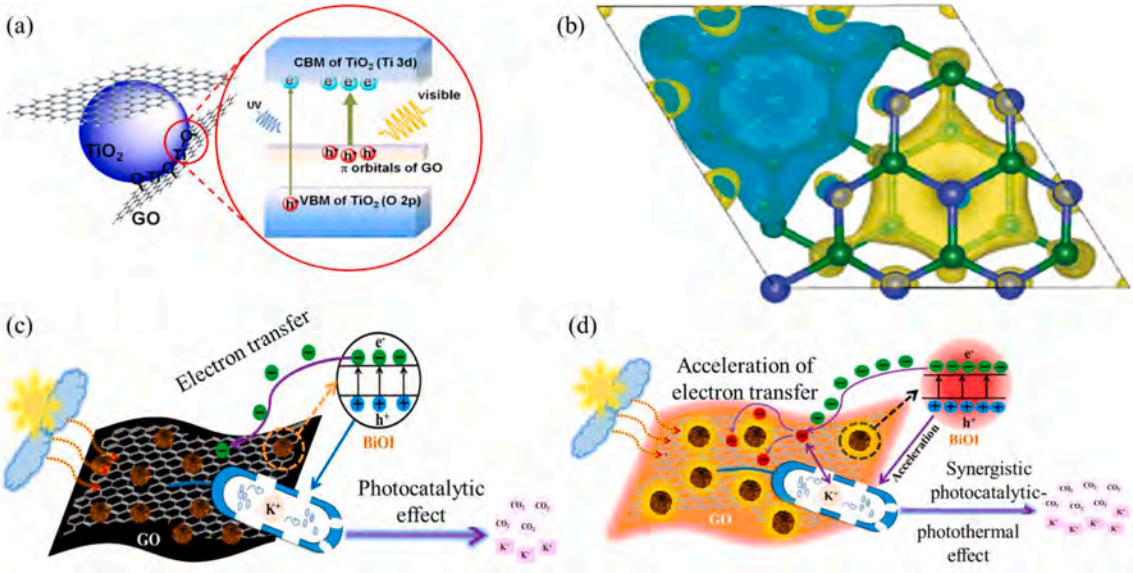

Fig. 4. (a) Ti–O–C bonding formed through interaction between unpaired π electrons on GO with surface Ti atoms of TiO_2. Reprinted with permission from Ref (Yeh et al., 2013). Copyright 2013, Elsevier. (b) Top view of the charge density difference plots at the graphene/g-C_3N_4 interface. Reprinted with permission from Ref (Du et al., 2012). Copyright 2012, American Chemical Society. Schematic illustration of possible antibacterial mechanism of (c) photocatalytic and (d) synergistic photocatalytic-photothermal process on BiOI-GO composite. Reprinted with permission from Ref (Yang et al., 2018). Copyright 2018, American Chemical Society.

role of rGO as an organic dye-like photosensitizer. However, their work didn't avoid the self-induced photosensitization effect of MB.

2.5. Photothermal effect

The photothermal effect (PTE) of graphene, has been experimentally reported to play a key auxiliary role in the enhancement of photocatalytic activity of graphene-based composite photocatalysts especially upon near infrared radiation (NIR) (Gan et al., 2014; Robinson et al., 2011). Although the temperature of the reaction mixture remains approximately constant, the graphene component of the composite photocatalyst still generates thermal energy continuously under photo-illumination thus promoting the transfer of the photogenerated carriers on the graphene sheet, keeping the photocatalytic reaction in a steady state regime and significantly improving the photocatalytic activity. However, very little is known about the inherent mechanism of PTE in graphene at present.

Gan's group firstly reported that not only did PTE of graphene exist but also its contribution was evaluated to be as high as ~37.6% in the entire photodegradation action of methylene blue (MB) by the P25 (TiO_2)-rGO nanocomposites (Gan et al., 2014). The enhanced degradation of MB might be ascribable to the following three points. (i) A higher carrier mobility of rGO sheets was expected at a higher local temperature of the rGO-P25 composite caused by PTE of graphene. (ii) The better photocatalytic activity was possibly related to the variation of the photoexcited efficiency in P25 with the rise of temperature. (iii) The hot carrier relaxation in graphene was unconnected with the temperature and then the carriers immediately have a hot distribution on account of the fantastic thermal conductivity of GO (Ruzicka et al., 2010). Considering the degradation of the industrially harmful and versatile dye, Oki's group developed graphene-polyaniline (GR-PANI) nanocomposites via acid-less method. Exposed to 808 or 980 nm NIR lasers in a concentration-dependent manner, the composites not only showed excellent photothermal stability and strong near-infrared (NIR) response but also generated a substantial amount of heat energy (Neelgund et al., 2016). Specially, under exposure to 980 nm laser for 7 min, the maximal temperature rise of 52.2 °C could be observed. In the study of Xue et al., CdS–Sn_2S_3 eutectic clusters structurally reconfigured irreversibly which was triggered off by the local PTE of graphene. Then these eutectic clusters tended to break into metal sulfides nanocrystals with ultrafine and tiny crystal size and were uniformly distributed on the rGO platform. Finally, an intimate and effective interfacial contact appeared (Xue et al., 2018). For killing of the bacterium *Acinetobacter baumannii* (*A. baumannii*), Yang et al. constructed BiOI/GO nanocomposite and explicitly investigated the phenomenon that photocatalysis and photothermal effect were mutually reinforcing. By contrast with the individual photocatalytic process in Fig. 4c, the synergistic photocatalytic-photothermal effect led to different sterilization processes to achieve more effective inactivation (Fig. 4d). In addition to conventional photocatalytic reactions driven by the sunlight irradiation, the PTE of GO also contributed a lot. Once the local temperature was raised, more efficient electrons would be excited and gained more energy to move faster. Conversely, the higher photothermal conversion effect was maintained ((Yang et al., 2018)).

In this section, we have critically discussed the roles of graphene in graphene-based composite photocatalysts. The cause of photocatalytic activity enhancement by combining with graphene can be revealed as following. Graphene's lower calculated Fermi level and high charge carriers mobility guarantee it as photoelectron transfer mediator; its different functional groups and delocalized π-electronic structure significantly enhance adsorptivity for reactants; its ability to narrow the band gap of semiconductors increase optical absorption range and intensity; its role as organic dye-like photosensitizer broaden visible light response without narrowing the band gap of semiconductors; its photothermal effect can generate thermal energy continuously particularly under NIR. Such summary about the origin of the activity enhancement in turn provides fundamental science to design agents developed based on graphene with higher photoactivities. However, just as unpredictable the performance of graphene-based photocatalytic systems is, the role of graphene in photocatalytic process is also still at issue.

3. h-BN: electron transfer or hole transfer?

2D hexagonal boron nitride (h-BN), as called "white graphene", is composed of boron and nitrogen atoms arranged in a sp^2 hybridized honeycomb-like lattice resembling graphene where the number ratio of B to N atoms is 1 to 1 (Song et al., 2012), featuring fantastic physicochemical properties such as high thermal conductivity, nontoxicity, low density and good chemical stability with excellent acid and oxidation resistance (Golberg et al., 2010). As an insulator with quite wide indirect band gap (5–6 eV) (Cassabois et al., 2016), it exhibits high thermal and chemical inertness and the optical absorption confined in deep ultraviolet range, which go against photocatalysis (Weng et al., 2015). On the other hand, considering its tunable band structure by introducing impurity defects and vacancy (Ataca and Ciraci, 2010), its higher specific surface area and larger adsorption capacity, BN is widely engineered as support matrix in photocatalytic application (Lv et al., 2016). Ball-milling, template and template-free method have been mainly used in preparing BN so far (Zhou et al., 2018c). Among these approaches, ball-milling method can achieve the scalability for mass production of h-BN. However, its oxidation-resistant and intercalation-resistant are the major challenges to prepare single or few layer materials. Recently, the photocatalytic performance would be enhanced after combing h-BN with the bulk semiconductors (Sheng et al., 2019). And it is of great value to further analyze the role of graphene-like BN in the photocatalysis.

3.1. Electron transfer

h-BN was previously reported to be a new sort of surface passivation material which could alter the behavior of photo-generated electron and suppress the combination of photogenerated h^+/e^- carriers (Shanmugam et al., 2013). Standing on that, Li's group simply synthesized BN/WO_3 composites via physical mixture i.e. the calcined method, promoting the surface photocatalytic degradation towards RhB but agglomerating severely (Xu et al., 2016). To overcome this problem, they then loaded successfully highly-dispersed WO_3 nanoparticles on the defective graphene-like BN nanosheets through an in situ one-step method (Yan et al., 2017). Due to the surface barrier passivation and the tight interface, the photo-generated electron transfer from WO_3 to BN came true. Recently, utilizing the key role of BN in electron transfer, bismuth-based semiconductor/BN hybrids with improved photocatalytic performance have emerged a lot, such as BN/BiOBr (Di et al., 2016), BN/$Bi_4O_5I_2$ (Ji et al., 2018), BN/BiOCl (Xu et al., 2017), BN/$BiPO_4$ (Chen et al., 2017). BN/BiOBr materials was prepared by Di and co-workers, where the photocatalytic activity of 1 wt% BN/BiOBr materials was the highest towards the removal of antibiotic agent (TC, CIP) and dye (RhB) (Di et al., 2016). From the SEM images of BN/BiOBr composite in Fig. 5a and Fig. 5b, a flower-like structure by nanosheet could be seen. Moreover, the BN on the surface of BiOBr indicated the successful coupling between BN and BiOBr. After the formation of tight contact interface between BN and BiOBr, photogenerated electrons on the CB of BiOBr could be effective strapped by BN to further activate molecular oxygen, which contributed advanced photocatalytic performance (Fig. 5c).

3.2. Hole transfer

The characteristic recombination time of photogenerated electrons is about 100 ns, which is not so short as that of surface holes (about 10 ns) (Hoffmann et al., 1995). It may be more essential to advance the transfer of holes, especially for the photodegradation reactions whose efficiency

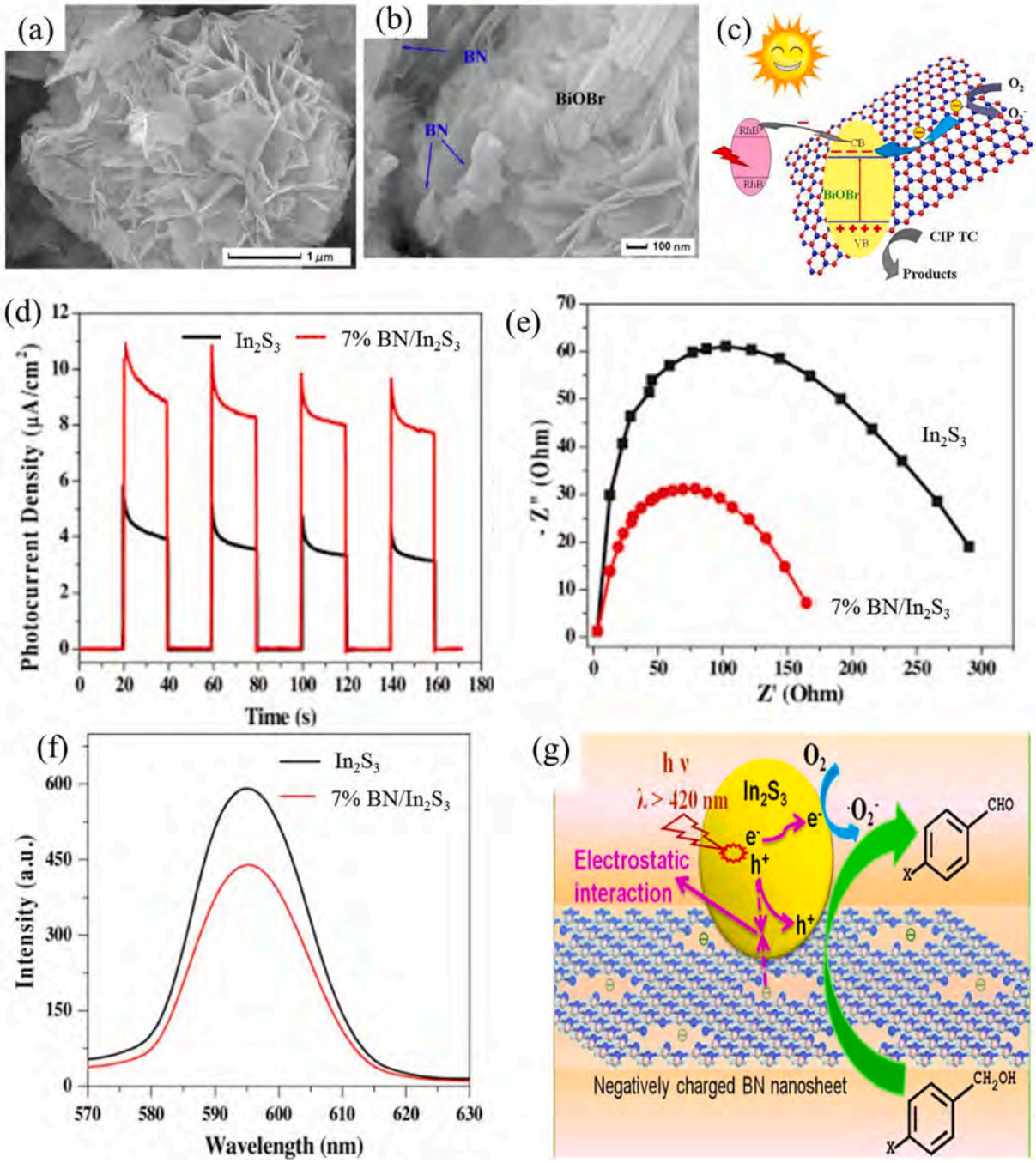

Fig. 5. (a) and (b) SEM images of 1 wt% graphene-like BN/BiOBr with flower-like structure. (c) Schematic of the separation and transfer of photogenerated charges in the graphene-like BN/BiOBr materials. Reprinted with permission from Ref (Di et al., 2016). Copyright 2016, Elsevier. (d) Transient photocurrent response of In_2S_3 and 7% BN/In_2S_3 composite under visible light irradiation. (e) EIS Nyquist plots of In_2S_3 and 7% BN/In_2S_3 composite. (f) PL spectra of pure In_2S_3 and 7% BN/In_2S_3 composite. (g) Proposed reaction mechanism for photocatalytic selective oxidation of benzyl alcohol over BN/In_2S_3 composite. Reprinted with permission from Ref (Meng et al., 2016). Copyright 2016, Elsevier.

is usually determined by the number of interfacial holes. Interestingly, ball-milled h-BN can be electronegative, wherein, the formation of nitrogen vacancies contributes chiefly (Meng et al., 2016). The negatively charged h-BN nanosheets is anticipated to attract the photoinducd holes as a hole transfer promoter to enhance the charge separation efficiency due to the electrostatic interaction, which is unlike graphene usually as electron transfer.

By coupling with the negatively charged h-BN, which conducted by the ball milling and acted as the hole transfer promoter, both the elevated photocatalytic activity and the suppression of the photocorrosion of ZnO were realized simultaneously (Fu et al., 2013b). Except ZnO, the facilitation of h-BN as hole transfer was also proved to be applicable to TiO_2 (Fu et al., 2013a). When coupled with a hole-capturer, the photocatalytic performance of metal sulfide would also be raised, such as In_2S_3 (Meng et al., 2016) and CdS ((Zhang et al., 2015)). Meng et al. prepared BN/In_2S_3 composite and studied its photocatalytic process for selective oxidation of several aromatic alcohols (Meng et al., 2016). While the weight ratio of BN to In_2S_3 was 7%, the composite photocatalysts possessed the best activity. According to the photoelectrochemical experiments, the photocurrent density was

remarkably enhanced in the 7% BN/In_2S_3 composite compared with pure In_2S_3 (Fig. 5d). On the other side, 7% BN/In_2S_3 composite had a smaller arc radius of the EIS Nyquist plot than that of pure In_2S_3 (Fig. 5e). Both consistently suggested the higher efficiency in the photoinduced electron-hole separation and the interfacial electron transfer with the introduction of BN. The photoluminescence (PL) measurement was further performed and a lower recombination rate of photoinduced carriers could also be concluded after the combination of In_2S_3 with BN nanosheets (Fig. 5f). The reaction mechanism was proposed that holes could migrate so quickly under the electrostatic attraction between the negatively charged BN and the photoexcited holes that the carrier pairs recombination was reduced (Fig. 5g).

For the photocatalysts, the charge transfer efficiency and the h^+-e^- recombination rate are two critical factors determining the photocatalytic activity. Coupling h-BN with semiconductors has been found to be valid to enhance the photocatalytic performance of semiconductors owing to their interfacial charge transfer properties. The key roles of h-BN were discussed in depth, while it is far from completion. BN can act as a kind of surface passivation material and transfer or accept photoexcited electrons from the CB of most semiconductors, which has been extensively reported. Interestingly enough, ball-milled h-BN can be negatively charged, supposed to boost the immigration of holes from the bulk of photocatalyst to its surface as a holes transfer promoter, which achieved the separation of photoinduced holes. The key roles of BN did enhance the photocatalytic activity.

4. g-C_3N_4: excellent metal-free semiconductor?

Graphitic carbon nitride (g-C_3N_4), the most stable allotrope among C_xN_y species, is a polymeric semiconductor with a graphene-like layered structure (Dong and Cheng, 2015). The metal-free nature endows g-C_3N_4 with environmental friendliness and the π-conjugated graphitic planes formed via polymerized tri-s-triazine units provide g-C_3N_4 with superior stability even in air up to 600 °C as well as in solutions with pH 0–14 (Thomas et al., 2008). Earth-abundance, the facile synthesis through pyrolysis of inexpensive precursors such as melamine, urea, cyanamide, dicyandiamide, thiourea or trithiocyanuric acid, and tunability of band gaps further contribute to its superiority (Shi et al., 2014; Zhang et al., 2012). As a good visible-light-active semiconductor (up to 460 nm) with a medium band gap (~2.7 eV), g-C_3N_4 possesses suitable band positions straddling the redox potential required for water splitting (Jiang et al., 2018d). In detail, the VB position (E_{VB}) and the CB position (E_{CB}) of g-C_3N_4 are about 1.57 and −1.13 eV, respectively (Hong et al., 2016). The former can trigger H_2 evolution and $\bullet O^{2-}$ production while the latter can induce water oxidation.

Desirable attributes as above render g-C_3N_4 an excellent metal-free semiconductor photocatalyst. Therefore, g-C_3N_4 has been widely researched and applied in all kinds of photocatalytic branches, such as selective photocatalytic oxidation (Bellardita et al., 2018), water splitting (Zheng et al., 2016), environmental remediation (Chen et al., 2017), and so on. However, pristine g-C_3N_4 is always restricted by its low specific surface area (2–10 m^2/g), marginal visible light absorption, ultrafast recombination photoexcited electron-hole pairs, and scarce charge mobility (Ding et al., 2018), resulting in unsatisfactory photocatalytic performance. Typically, recent research revealed that photoelectrons, deep trapped in g-C_3N_4 and having no reactivity for proton reduction, would seriously hinder the accumulation of holes and depress hydrogen production (Godin et al., 2017). Tremendous efforts have been payed to improve the photocatalytic performance of g-C_3N_4 and several main modification strategies can be cited hereinbelow. (i) Heterojunction construction. Heterojunction-type photocatalytic systems formed by the coupling of two semiconductors with well-matched energy levels can successfully separate the photoinduced electron (e^-)-hole (h^+) pairs due to the potential differences on their CB and VB (Chen et al., 2017a; Guo et al., 2018, 2021a) (,). Homogeneous and stable, isotype g–C_3N_4–based heterojunctions are more fascinating than the allotypic one (Liu et al., 2017; Tong et al., 2016)(;). By a unique microwave-assisted molten-salt (mw-ms) process, Liu et al. prepared an isotype heterojunction of triazine-/heptazine based g-C_3N_4 hybrids ((Liu et al., 2017)). The huge improvement in photocatalytic H_2 evolution efficiency could be attributed to the construction of type II heterojunction in as-prepared sample, which depressed the charge recombination. Unfortunately, the redox ability of photogenerated charges is inevitably lowered to some extent after the charges transfer in such system. Our group synthesized g-C_3N_4 based direct dual Z-scheme ternary composite photocatalyst (WO_3/g-C_3N_4/Bi_2O_3), which not only promoted the fast separation of photogenerated charges but also retained prominent redox ability for photodegradation of TC (Jiang et al., 2018a). Especially, we also comprehensively overviewed the design, preparation, and applications of the artificial all-solid-state g–C_3N_4–based Z-scheme photocatalysts which simulates natural photosynthesis (Jiang et al., 2018b). Besides, the study of heterojunction-type photocatalytic systems based on g-C_3N_4 has made remarkable achievements in theory. Adopting DFT approach, Liu's group calculated energy band structure and investigated the interfacial interaction of g-C_3N_4/CdS heterostructure (Liu, 2015). Once g-C_3N_4 contacted with CdS, the calculated band edge potentials (CB and VB) varied with the Fermi level and then formed a type-II heterostructure. (ii) Nano-structural engineering. Nanostructured photocatalysts can elevate the photocatalytic performance which could not be achieved by traditional bulk counterparts, benefiting from larger specific surface area and the shorter diffusion pathways. Porous g-C_3N_4 nanosheets (Fig. 6a) where the photoexcited electrons and holes can migrate to their surface with ease earned profoundly increased photocatalytic performance compared with bulk g-C_3N_4 where charge carriers are prone to recombination (Fig. 6b) (Huang et al., 2017). Another "seaweed" nanostructured g-C_3N_4 also showed high H_2 evolution (Han et al., 2015). Such seaweed-like g-C_3N_4 with mesoporous structure (Fig. 6c) possessed a better electron-transfer and light-harvest ability. Tong et al. prepared thylakoid-bioinspired multishell g-C_3N_4 nanocapsules (Fig. 6d), which were provided with the porous thin shells and hollow lumens. Profiting from the nanoarchitectures, the incident light would be repeatedly scattered and refracted (Fig. 6e). Finally, superior photocatalytic performance for H_2 generation was exhibited due to the stronger visible-light harvesting and faster electron transfer (Tong et al., 2017). (iii) Element doping. By deliberately incorporating impurities, the electronic structure of g-C_3N_4 can be modulated at the atomic level, which makes its redox potential and optical absorption ability controllable. Regarding that element doping was an efficient modification strategy, we gave a review before on the recent progress in the development of doped g-C_3N_4 systems for photocatalysis (Jiang et al., 2017a). Typically, our group co-doped g-C_3N_4 with P and S for enhanced degradation towards TC and MO. We deemed that introducing more defects as the trapping centers of photo-generated electrons into the framework is favorable for the separation of photoinduced charges (Jiang et al., 2017b). Considering that g-C_3N_4 was a layered material and had interlayer galleries, doping by intercalation modification appeared to be a new promising orientation. K atoms (Xiong et al., 2016), Cl atoms (Liu et al., 2017) and Sr atoms (Li et al., 2018), intercalated into the interlayer space of g-C_3N_4, were all afforded to establish interlayer channels and benefit the carriers transport and separation. Besides, heterojunction or nanoengineering based on doped g-C_3N_4 has been achieved by our research group. Phosphorus-doped g-C_3N_4/g-C_3N_4 isotype heterojunctions (Jiang et al., 2018c), carbon-doped g-C_3N_4/$Bi_{12}O_{17}Cl_2$ heterojunctions (Zhou et al., 2018b), nitrogen self-doped g-C_3N_4 nanosheets (Jiang et al., 2019) and highly porous carbon doped g-C_3N_4 (Zhou et al., 2018a) all adopted "two-in-one" strategy and elevated visible-light photocatalysis. (iv) Copolymerization. As a form of molecular doping, copolymerization is ordinarily reached by mixing another organic monomer with the precursor during the synthesis of g-C_3N_4, which can regulate its π-conjugated aromatic system, band structure, and photoactivity. Very recently, benzene-ring

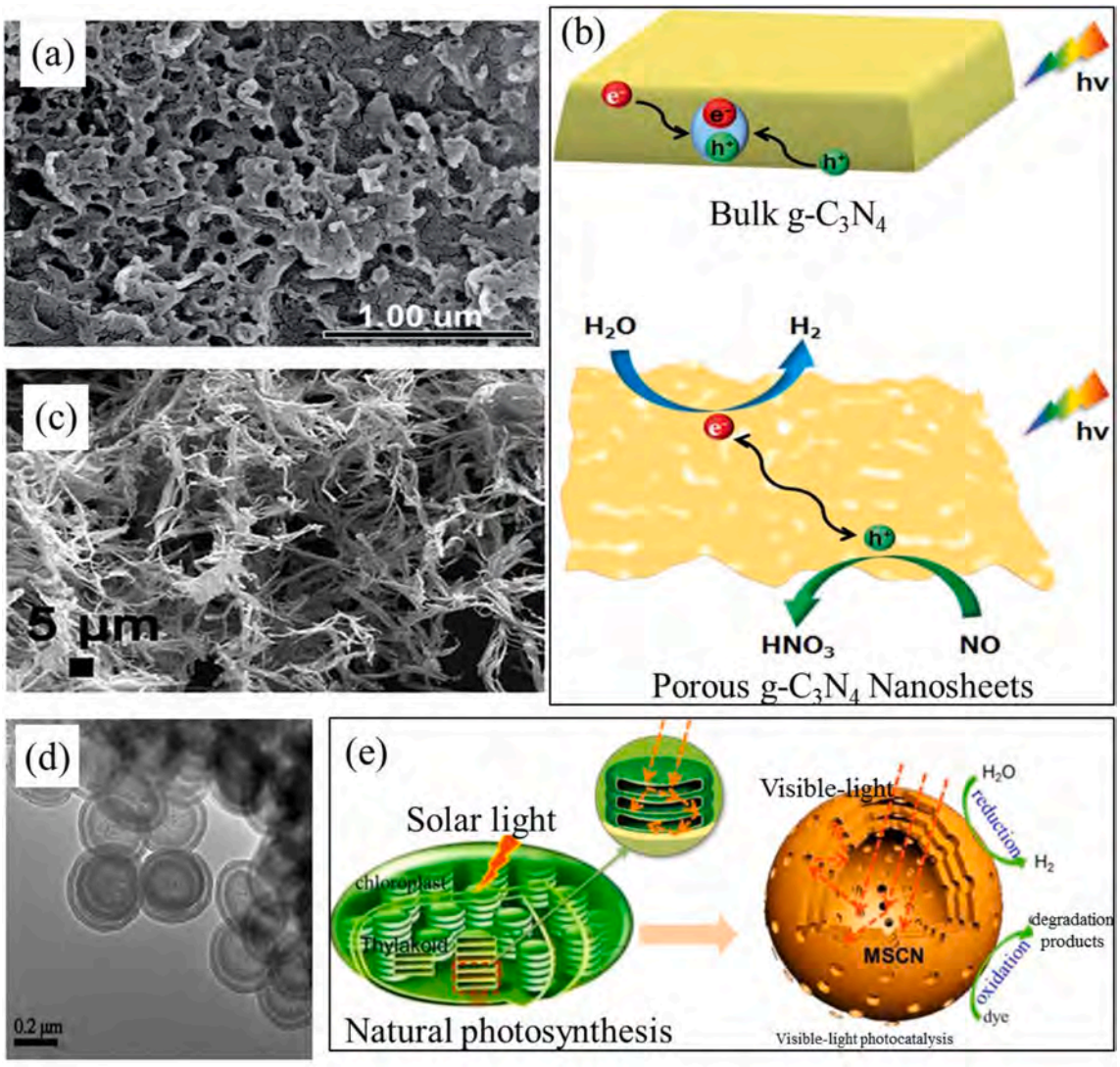

Fig. 6. (a) SEM images of porous g-C_3N_4. (b) Diagram for charge separation of bulk g-C_3N_4 and porous g-C_3N_4 nanosheets. Reprinted with permission from Ref (Huang et al., 2017). Copyright 2017, The Royal Society of Chemistry. (c) Low-magnification SEM images of the freeze-dried, hydrothermally treated dicyandiamide (HTD). Reprinted with permission from Ref (Han et al., 2015). Copyright 2015, Wiley. (d) TEM images of MSCN nanocapsules. (e) Schematic diagram showing the photocatalytic reaction over MSCN photocatalyst under visible light irradiation. Reprinted with permission from Ref (Tong et al., 2017). Copyright 2017, American Chemical Society.

doped g-C_3N_4 photocatalysts were prepared by two main steps. Urea and 4, 4′-sulfonyldiphenol (BPS) were carried out the thermal co-polymerized first and then treated with a heat-etching step (Liu et al., 2019). A narrower band gap from 2.7eV to 2.33eV, more harvest of visible-light photons and more effective separation of carriers caused 12-fold improvement of H_2 production than that of pristine g-C_3N_4 nanosheets. (v) Dye sensitization. Coloured dyes like MO, MB, RhB, etc. can work as a valid visible-light absorbing molecule and involve dye sensitization effect to expand the light response range of g-C_3N_4 (Patnaik et al., 2018). As fluorescein has a stronger electron transfer ability from its LUMO to g-C_3N_4 than other dyes, Qin et al. selected it to serve as a photosensitizer to enhance the photocatalytic activity of g-C_3N_4 (Qin et al., 2016). In the presence of fluorescein, H_2 production showed a steep rise to 2014.20 μmol g^{-1} h^{-1} which was even approximately 4.8 times as high as that of the g-C_3N_4 with 3 wt% Ag loading.

To sum up, g-C_3N_4 has been a bright photocatalyst thanks to its particular layered structure, metal-free nature, biocompatibility, nice chemical and thermal stability, simple fabrication, desirable visible-light response and appropriate band positions. Most of all, the electronic features and the tunable structure of g-C_3N_4 allow for easy modifications to overcome its shortcomings. Heterojunction construction by coupling g-C_3N_4 with other semiconductors can effectively promote charge transfer and separation. Nano-structuring g-C_3N_4 with specific morphologies can afford large surface area and short diffusion pathways to optimize photocatalytic activity. Modulating the band structure of g-C_3N_4 at the atomic level (like elemental doping) and the molecular level (like copolymerization) can obtain better light-harvesting ability or stronger redox ability. The dye sensitization effect tends to be employed to broaden light response region of g-C_3N_4. These modification strategies make it possible for g-C_3N_4 to be an excellent photocatalyst.

5. Black phosphorus: a photocatalyst or co-catalyst?

Black phosphorus (BP), the most thermodynamically stable allotrope of phosphorus (P), emerged as a new 2D metal-free semiconductor with a graphene-like layered structure in early 2014 (Liu et al., 2014). The common top-down method for the fabrication of BP can realize mass-production, however, the obtained materials are not crystallized and a great deal of organic solvent will be consumed, boosting the

budgets of preparation invisibly. Wet-chemical self-assembly and CVD are reported with lower cost but excellent crystallization, meaning these bottom-up methods should be developed full blast. BP features a puckered honeycomb structure where interlayers are stacked together by weak van der Waals interactions and each in-plane phosphorus atom covalently bonds to three nearest neighbors via sp^3 hybridization (Hultgren et al., 1935; Zhang et al., 2019). This atomic arrangement yields armchair- and zigzag-shaped structure parallel and perpendicular to the atomic ridges, respectively (Jang et al., 2015). Its hole mobility equals as high as 1000 $cm^2 V^{-1} s^{-1}$ (Li et al., 2014). In some cases, the properties of BP for photocatalysis are deemed to outperform even those of graphene. The so called "wonder material" graphene fails to act as a semiconductor and a qualified photocatalyst due to its zero intrinsic band gap, which arouses a low ON/OFF ratio (ca. 5.5–44) (Jain et al., 2017). By contrast, the direct band gap of BP decreases with the increase of 2D layers as displayed in Fig. 7a (Batmunkh et al., 2016). The tunable bandgap spans from 0.3 eV for bulk to 2.0 eV for a single layer, which enables BP to hold broad light response from UV to visible and even NIR region (Tran et al., 2014). Serendipitously, BP bridges the existing gap between graphene and other 2D materials (Fig. 7b) (Castellanos-gomez, 2015). Furthermore, BP exhibits favorable current ON/OFF ratio (ca. 10^4–10^5), strong intrinsic in-plane anisotropy and much higher specific surface area due to its puckered lattice configuration (Li et al., 2014). These remarkable properties testify that BP is becoming a "rising star" of post-graphene 2D metal-free photocatalyst.

Easily adjustable bandgap and high charge mobility guarantee the wide application of BP as one broad spectrum photocatalyst in the field of photocatalysis, especially for water splitting. By ball-milling bulk BP, the potential of BP nanosheets for photocatalytic H_2 evolution using visible light was shown in Zhu's study (Zhu et al., 2017). It's a pity that rapid charge recombination retarded the photocatalytic efficacy of bare BP nanostructure. Coupling BP with other metals or semiconductors was recognized as an effective solution to avoid recombination. Majima's group prepared ternary BP/Pt/rGO nanocomposite, whose optimum H_2 evolution rates reached to ca. 0.84 mmol $g^{-1} h^{-1}$ and 3.4 mmol $g^{-1} h^{-1}$ upon >780 nm and >420 nm illumination, respectively (Zhu et al., 2017b). In this system, Pt/rGO contributed to a reduced charge recombination while 2D BP nanoflakes acted as a photocatalyst for harnessing visible and NIR light. The photoelectrons in the CB of BP could be injected into rGO nanosheets next to be captured by Pt and then H_2 generation occurred (Fig. 8a). Whereas noble metal like Pt was usually limited-reserves and high-price, they subsequently developed BP/WS_2 hybrid as a noble metal-free NIR-driven photocatalytic H_2 production system (Zhu et al., 2018b). In the existence of WS_2, the CB electrons could be injected from excited BP to WS_2 nanoflakes, which was of significance for promoting charge separation and electron reductive reaction (Fig. 8b). Furthermore, by designing a new artificial Z-scheme heterostructure of 2D/2D BP/$BiVO_4$, they made it feasible that overall water splitting was conducted without any addition of sacrificial agents and external bias (Zhu et al., 2018a). The respective band structures with a staggered alignment made possible the effective charge separation, which allowed H_2 and O_2 evolution to come about on BP and $BiVO_4$, respectively.

The addition of co-catalysts has been identified as one of typical strategies to improve the sluggish surface reaction kinetics (Wang et al., 2018). Transitional metals like noble-metal Pt are currently widely applied as co-catalysts. Nonetheless, metal-based co-catalysts are usually unfriendly to environment, costly and limited. In contrast, the aforementioned prominent properties show BP as a potential high-performance metal-free co-catalyst: (1) outstanding hole mobility; (2) tunable band gap; (3) ultrahigh specific surface area. Based on both experimental and theoretical results, Ran's group successfully demonstrated the application of BP as a universal and efficient nonmetallic co-catalyst for CdS (CS), $Zn_{0.8}Cd_{0.2}S$ (ZCS) and ZnS (ZS) (Ran et al., 2017). First, instructed by density functional theory (DFT) calculations, they studied the relationship between the bandgap of BP and its layer number. The computation results indicated quad-, tri-, bi- and monolayer corresponded to the band gap of 1.400, 1.525, 1.643 and 2.020 eV, respectively, while the band gap of bulk BP was 0.317 eV. Then they experimentally integrated bulk BP, BP nanosheet for 10–14 layers (BPS) and few layer phosphorene nanosheet for 5–6 layers (FPS) with different metal-sulfides (CS, ZCS and ZS). Theoretical and experimental studies are consistent with the results that the less layer number of BP led to the better photocatalytic activity in all composite systems. And the photocatalytic performance and mechanism of FPS/CS system were thoroughly studied in Fig. 8c. Since the E_F position of FPS is lower than that of CS, the photo-excited electrons would migrate from the main photocatalyst CS to the co-catalyst FPS upon visible-light illumination, thus separating carrier pairs. Due to the high charge mobility of FPS, electrons then rapidly moved to its massive active centers for participation in H_2 evolution. For another photocatalyst composited of $Zn_{0.5}Cd_{0.5}S$ and 2D BP nanosheets, BP acted as co-catalyst which successfully extended the absorption spectrum of the composites to the wavelength above 510 nm (Fig. 8d) (Zhao et al., 2018). Obviously, it was demonstrated that this BP co-catalyst in different metal-sulfide systems had the huge generality.

Above all, we have briefly summarized the characteristics of BP and highlighted its superior semiconductor performances beyond graphene,

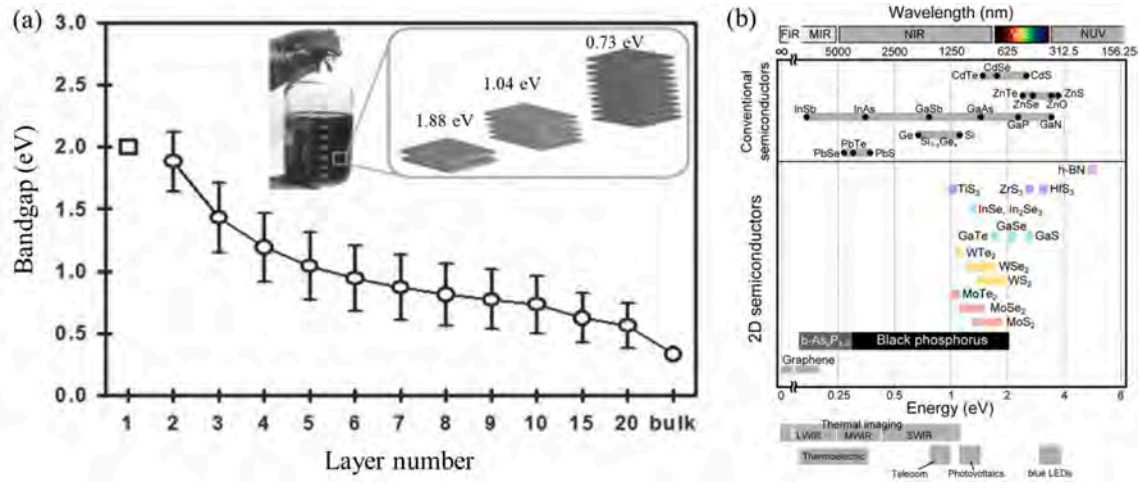

Fig. 7. (a) Energy bandgap of phosphorene with different thicknesses. Reprinted with permission from Ref (Batmunkh et al., 2016). Copyright 2016, Wiley. (b) Comparison of the band gap values for different 2D semiconductor materials. Reprinted with permission from Ref (Castellanos-gomez, 2015). Copyright 2015, American Chemical Society.

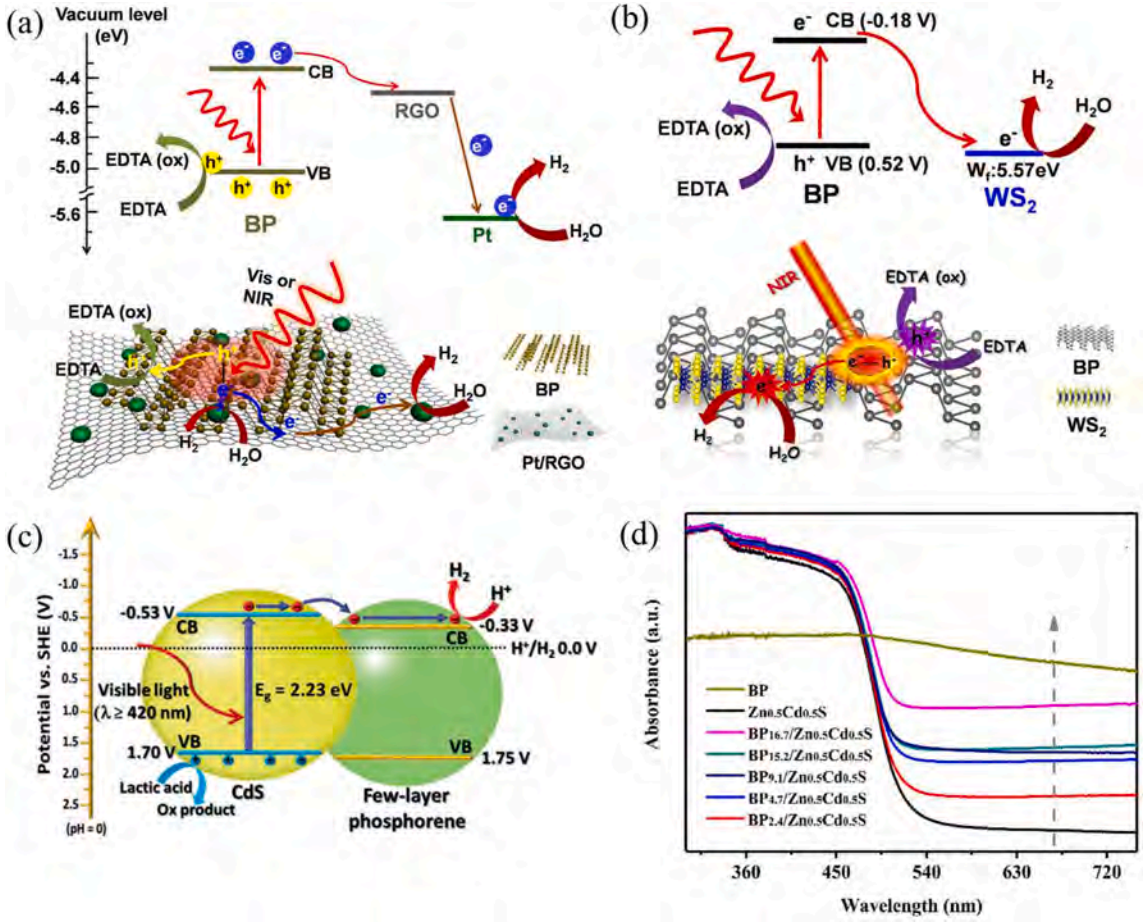

Fig. 8. (a) Proposed schematic diagram and reaction mechanism for the visible and NIR light activated photocatalytic H_2 evolution of 2D BP nanoflakes and Pt/RG. Reprinted with permission from Ref (Zhu et al., 2017b). Copyright 2017, Elsevier. (b) Proposed schematic diagram for the NIR light activated photocatalytic H_2 production of BP/WS_2 hybrids in the presence of EDTA. Reprinted with permission from Ref (Zhu et al., 2018b). Copyright 2018, Elsevier. (c) Illustration of the photocatalytic mechanism of FPS/CS system under visible-light irradiation. Reprinted with permission from Ref (Ran et al., 2017). Copyright 2017, Wiley (d) The UV–vis diffuse reflection spectrum. Reprinted with permission from Ref (Zhao et al., 2018). Copyright 2018, Wiley.

including its adjustable thickness-dependent direct band gap, favorable current ON/OFF ratio, fantastic intrinsic in-plane anisotropy, higher specific surface area along with excellent hole mobility. On the basis of these features, especially the bandgap tunability in the range of 0.3–2.0 eV, BP possesses the wide application as one broad spectrum photocatalyst which can absorb visible and near-infrared light for photocatalytic H_2 evolution. By tuning the thickness of BP, it is also to achieve a promising co-catalyst for extending photocatalytic energy conversion to the visible and NIR regions. However, to turn BP into the most valuable material in the post-graphene era, most of the breakthroughs are still to come.

6. COFs: potential metal-free semiconductor?

Covalent organic frameworks (COFs), a novel class of graphene-like crystalline porous conjugated polymers constructed solely with light elements (C, H, O, N and B) by strong reversible covalent bonds, have been of particular interest since the synthesis and application of COFs was pioneered in 2005 (Co et al., 2005). COFs are synthesized by reversible condensation reactions under thermodynamic control, whose linking groups are usually boronates, boroxines (Co et al., 2005), triazines (Kuhn et al., 2008), imines (Dalapati et al., 2015), or hydrazones (Stegbauer et al., 2014). In this context, COFs are metal-free and cost-efficient, which is expected to meet the requirements of industrial applications. Different from g-C_3N_4 which has finite chemical varieties for structural optimization due to the invariable composition of heptazine or triazine units, COFs feature structural periodicity and a predictable, long-range order of building blocks, which make it possible precisely tunable framework topologies with adjustable functional design (Schwarz et al., 2019). More specifically, its physicochemical properties and band structure can be tailored by judicious selection of building units, linkage motifs, and their stacking mode (Sick et al., 2018). Based on this, the semiconducting properties inherent to COFs which can obtain by using appropriate functional molecules in its synthesis process rival that of g-C_3N_4 and metal-organic frameworks (MOFs) (Stegbauer et al., 2018). Moreover, 2D-COFs are remarkably characterized by periodic columnar π-arrays arising from layered π-stacking of 2D polymer sheets in a face-to-face way (Yang and Wei, 2016). These ordered columns provide defined channels for charge-carrier diffusion, migration and separation, which benefits 2D-COFs a lot in the application as organic semiconductors for heterogeneous photocatalysts (Ding et al., 2011). Combining three crucial features related to the photocatalytic process, namely tunability, crystallinity and porosity, COFs are becoming ideal metal-free flexible photocatalysts (Chen et al., 2019).

Different kinds of semiconductor characteristics can be bestowed on COFs by carefully selecting monomers as the building blocks. Choosing electron-withdrawing building blocks (e.g., benzothiadiazole) usually obtain ambipolar or n-type semiconductors, whilst integrating building blocks with rich conjugated Π-electron (e.g., tetrathiafulvalene) can switch them to p-type semiconducting COFs (Yang and Wei, 2016). Therefore, investigations on the potentiality of COFs pertaining to

heterogeneous semiconductor photocatalysis are under serious consideration, especially their capable of photocatalytic hydrogen evolution. Lotsch and co-workers have done a great deal of work on this project (Banerjee et al, 2017, 2018; Stegbauer et al., 2018; 2014; Vyas et al., 2015). The first COF to be photoactive in hydrogen evolution under visible light irradiation was reported by them in 2014 (Stegbauer et al., 2014). The hydrazone-linked COFs consisted of phenyl and triazine building blocks and presented a 2D layered structure with the in-plane honeycomb lattice. It featured a bandgap of 2.8 eV, 3.8 nm-diameter mesopores and a larger specific area of 1603 $m^2 g^{-1}$. In the presence of a sacrificial donor of TEOA and a proton reduction catalyst of Pt, the well-ordered model system, Pt-modified COF showed higher H_2 production of 1970 μmol h^{-1} g^{-1} for first 5 h. To disclose the significant impact of the molecular building blocks modification on photocatalytic H_2 production efficiency of COFs, they further synthesized four 2D azine-linked COFs with a nitrogen-atoms number variation in the central aryl ring from 0 to 3 (Fig. 9a) (Vyas et al., 2015). A stepwise increase in the N content and hence the planarity could lead to the increase in porosity and crystallinity. In N_3–COF, the higher number of N atoms contributed to not only extending π-delocalization through the enhanced planarization but also optimizing the photocatalytic activity by retarding the charge recombination via fast electron migration. Another three azine-linked COFs from pyrene building blocks were presented by them recently and the nitrogen content of these COFs was different. It was in the peripheral aromatic units instead of the central ring that the number of nitrogen atoms varied (Stegbauer et al., 2018). In comparison with the aforementioned azine COF samples, relative activities of the three all-planar and conjugated COFs didn't depend on their geometrical structures but their composition and electronic properties. And the thermodynamic driving force for H_2 evolution had negative correlation with the number of N atoms of COFs. Given that platinum co-catalyst was always used to cut down the overpotential for H_2 reduction, they developed a non-noble-metal, single-site heterogenized photocatalytic H_2 generation system by combining COFs with molecular cobaloximes co-catalysts (Banerjee et al., 2017). Efficient H_2 evolution would be seen in the system using N2–COF photosensitizer, cobaloxime proton reduction co-catalyst (Co-1), TEOA sacrificial electron donor, where both kinetics and thermodynamics of the charge-transfer processes between COF and co-catalyst play a decisive role. Also, the group reviewed the advances of COFs photocatalysts for H_2 evolution not long ago (Banerjee et al., 2018). Other interesting photocatalytic applications in CO_2 reduction (Yang et al., 2018), decomposition of organic pollutants (He et al., 2017), selective oxidation (Huang et al., 2017), organic transformations (Zhi et al., 2017) and more were also found.

However, the structural periodicity in an identical COF skeleton will lead to limited building units, which is hard to simultaneously meet all these key points for improving photocatalytic activity, namely strong photo-absorption, high charge-separation efficiency, large surface area, as well as long-term stability. Forming proper composites which could create synergistic effect may afford these multifunctional properties. Through deliberate design, conjugating metal-organic frameworks (MOFs) with COFs can provide more possibilities for maintaining porosity, crystallinity, stability and the opposite migration of photoinduced electrons and holes for carrier separation (Peng et al., 2018; Zhang et al., 2018). Given that weak interaction (hydrogen bonds or Van der Waals forces) is the most common connectivity combination modes between COF and another component in COF-based hybrids, Lan's group first successfully integrated 2D TpPa-1-COF with stable MOF (NH_2-UiO-66) by strong connection of covalent bonds (Zhang et al., 2018). The resulting NH_2-UiO-66/TpPa-1-COF hybrids were prepared via introducing the former into the synthesis reaction system of the latter

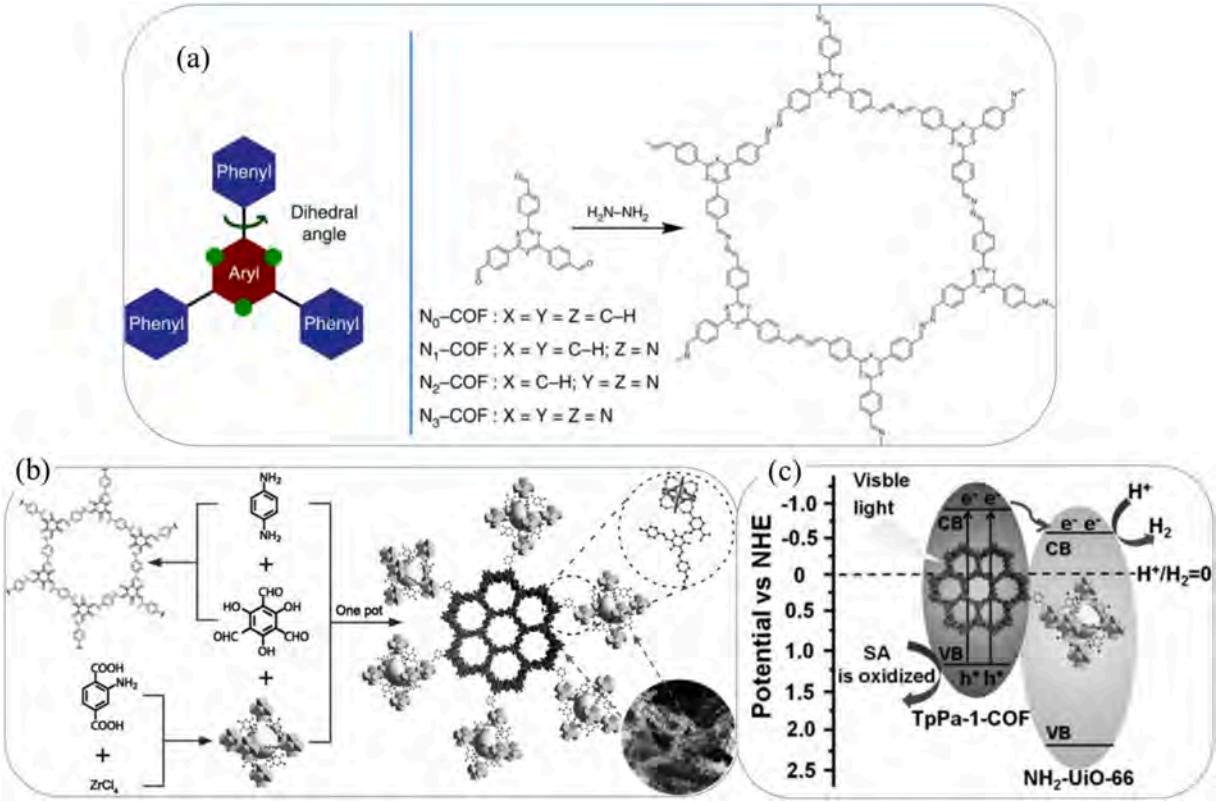

Fig. 9. (a) A substitution of alternate carbons in the central aryl ring of the triphenylaryl platform (green dots) by nitrogen atoms and synthesis of Nx–COFs from Nx–aldehydes and hydrazine. Reprinted with permission from Ref (Vyas et al., 2015). Copyright 2015, Springer Nature. (b) Schematic illustration of the synthesis of NH_2-UiO-66/TpPa-1-COF hybrid material. (c) Mechanism schematic of NH_2-UiO-66/TpPa-1-COF (4:6) hybrid material. Reprinted with permission from Ref (Zhang et al., 2018). Copyright 2018, Wiley. (For interpretation of the references to colour in this figure legend, the reader is referred to the Web version of this article.)

(Fig. 9b). In the ultra-high H_2 evolution process of the hierarchical porous hybrid materials, TpPa-1-COF played an effective light-harvest role under visible light irradiation, and then well-matching band gaps between the two species guaranteed the efficient charge separation through covalent connecting junction (Fig. 9c). On the other side, though COFs are constructed entirely from covalent bonds, their chemical stabilities and electron delocalization remain to be further amplified. It can be illustrated by the bottleneck that imine-based COFs tend to suffer hydrolysis in an acidic environment owing to the dynamic nature of imine bond (Li et al., 2018). Forming stable fully conjugated imine-free COFs with sp^2-carbon double bond structures is being actively exploring. Wang et al. successfully oxidized amines to imines in visible-light irradiation and aerobic condition by a 2D Por-sp^2c-COF system, where porphyrin was selected as functional molecule and COFs were linked by sp^2 carbon (Wang et al., 2019). Under the same photocatalytic reaction condition, imine-linked Por-COF was totally decomposed due to the low chemical stability, whilst Por-sp^2c-COF exhibited interesting photocatalytic activity, comparable to some heterogeneous metal-based photocatalyst. Benefitting from the nature of C═C linkages, Por-sp^2c-COF could be stable even in solutions like 9 M NaOH and 9 M HCl or in air up to 250 °C.

The past decades have witnessed progress in photocatalysis that the concept of controllability is gradually introduced into the design philosophy of photocatalyst, making the preparation process more directive and efficient. The exceptional blend of solid-state trait together with semiconducting property, modularity, porosity, crystallinity, rigidity and stability means that COFs have great potential to be avant-garde in photocatalysis research. Particularly, its capable of photocatalytic hydrogen evolution has been largely demonstrated. COFs also provide an ideal scaffold to anchor photocatalytically active nanoparticles due to its π-conjugated backbones and large surface area, which can be exemplified by the deposition of CdS nanoparticles on an extremely stable 2D COF support for H_2 evolution (Thote et al., 2014). In COFs-based photocatalysts, COFs usually act as photoabsorber, photosensitizer, electrons transfer mediator and acceptor. However, above results mark just the beginning of a prospering area of COFs as photocatalysts, whose every aspect needs to be scrutinized to push the limits of COFs photocatalysis further.

7. Hybrid metal-free 2D photocatalysts

The hybridization of 2D metal-free materials is highly promising to realize admirable photocatalytic performance by combining their notable merits. There exist some advantages: (i) the distinct “face to face” contact creates large interface area and robust interactions for reducing the charge transport distance and time, to promote interfacial charge separation and transfer between layers (Low et al., 2014); (ii) the strong electronic coupling between layers optimizes electronic structure (Zheng et al., 2014); (iii) the composition of various 2D materials with different bandgap width can cover a broad light-responsive range; (iv) the huge potential and versatility by selecting and combining different 2D materials enable unprecedented flexibility in controlling the chemical reactivity (Fu and Bao, 2017; Geim and Grigorieva, 2013). On the other hand, metal-containing photocatalysts suffer from problems such as limited reserves, high economic cost for large-scale production, and hazardous environmental impact. In the drive toward sustainable development, it is greatly desirable to develop metal-free photocatalysts. A list of some 2D/2D hybrid systems based on above GMFs is summarized in the Supporting Information (Table S1).

Notably, the analogous carbon network and sp^2-bonded π-structure endow graphene and g-C_3N_4 the compatibility to be easily combined as a photocatalyst (Li et al., 2013). The hybridization of g-C_3N_4 with graphene will overcome the disadvantages of each component, which has sparked incessant interest (Ong et al., 2015a; Sun et al., 2017). Ong et al. adopted rGO as a structure-directing agent and fabricated sandwich-like rGO/g-C_3N_4 (GCN) nanocomposites to convert CO_2 into CH_4. The formation of *C*–O–C bonds for cross linking caused a slight absorption red shift (Ong et al., 2015a). Also, graphene acted as a great scaffold to storage electron and prevented the electron−hole pairs of g-C_3N_4 from recombining. In another work by the similar research group, they adopted the sonication-exfoliation of HCl-acidified bulk g-C_3N_4 strategy and obtained protonated g-C_3N_4 (pCN). 2D/2D rGO/pCN nanostructures were further constructed though π–π stacking interaction as well as electrostatic attraction between electronegative rGO and electropositive pCN (Ong et al., 2015b). Both exceptional 2D/2D morphological structure and adequate intimate interfacial coupling after surface charge modification between rGO and pCN contributed to the remarkably improved photoredox processes, thereby successfully harnessing rGO as the photogenerated electron reservoir to accelerate the charge transfer and separation over rGO/pCN.

Apart from 2D graphene-g-C_3N_4 hybrids, other hybrid nonmetal 2D photocatalysts have been developed, including BN/g-C_3N_4 (Gu et al., 2017; Jiang et al., 2018d), BP/g-C_3N_4 (Ran et al., 2018), graphene/h-BN (Li et al., 2017), graphene/BP (Zhang et al., 2019), graphene/COFs (Li et al., 2016), g-C_3N_4/COFs (Luo et al., 2019) and so on. In the BN/g-C_3N_4 composites photocatalytic system, BN mainly functioned in enlarging surface areas for reactant adsorption, passivating the surface barrier as electrons transfer, or altering the behavior of holes. Interestingly, the quite reactive (002) facet edge of BN is also capable of providing reactive catalytic sites, though hardly reported in photocatalytic fields (Lv et al., 2016). Based on that, Gu et al. modified 2D g-C_3N_4 with BN terminated by –OH groups to construct a novel metal-free photocatalyst (Gu et al., 2017). BN not only altered the behavior of holes by electrostatic interactions, but also acted as catalytic sites for oxygen activation. Besides, a binary nanohybrid (BP/g-C_3N_4) was observed that the photocatalytic H_2 production efficiency was both significantly enhanced with visible and NIR light irradiation (Zhu et al., 2017a). Driven by $>$ 420 nm light, BP could act as the electron sink and accepted electrons to its conduction band. While driven by $>$ 780 nm light, photoelectrons would be trapped in the interfacial P–N coordinate bond of BP/CN. The average lifetime of such electrons was both prolonged. As for graphene/COFs hybrids, Li’s group constructed graphene/g-$C_{12}N_7H_3$ heterojunction (Li et al., 2016). Holes in the VB of g-$C_{12}N_7H_3$ could be trapped because of the formation of Schottky barrier ($\varphi sb = 1.05$ eV), whereas electrons freely diffused from the CB of g-$C_{12}N_7H_3$ to graphene, thus an effective separation of photoexcited charge carriers occurred.

8. Conclusion and perspectives

Due to their distinctive peculiarities like high aspect-ratio, large surface-to-volume ratio, excellent biocompatibility and biosafety, adequate surface groups and developed porosity, remarkable progress has been made in the photocatalytic research fields of above GMFs and their composites. This review addressed the achievements of GMFs from the points of fundamental features and their roles in enhancement of photocatalytic activity. Photocatalysis-related properties of 2D materials are presented in Fig. 10. Although there are the same 2D feature and analogies in their lattice structures, such GMFs possess diversity in mechanical, thermal, electrical, optical and catalytic properties. Graphene is superior as it owns the highest charge carrier mobility, but fails to function as a semiconductor due to the absence of bandgap in its electronic structure. Compared with graphene, h-BN possesses an ultrawide bandgap (5–6 eV), a larger specific surface area and better adsorption capacity. With the puckered lattice structure, the mechanical strength of BP is largely weakened. Simultaneously, this characteristic results in unique anisotropy. Particularly, BP holds a unique advantage that its direct-bandgap can be tuned sufficiently for broadband absorption, while preserving wonderful charge mobility that surpasses the graphene. Distinguishing from inorganic semiconductors, organic counterparts are intriguing on account of unlimited choices of various building blocks, versatile modification of material composition and properties, and diverse synthetic modularity. Graphitic carbon nitride

Key photocatalysis-related properties of 2D metal-free materials

	Graphene	h-BN	g-C_3N_4	BP	COFs
Mechanical properties	sp^2 hybridization tensile strength of 130.5 GPa Young's modulus of 1.0 TPa a fracture toughness of ~4 MPa·m$^{1/2}$	sp^2 hybridization tensile strength of ~70.5 GPa Young's modulus of 0.2-0.8 TPa	π-conjugated polymer semiconductor sp^2 hybridization two phases, the striazine-based C_3N_4 (s-C_3N_4) and triazine-based C_3N_4 (t-C_3N_4)	structural anisotropy sp^3 hybridization Young's modulus of 0.035-0.166 TPa	composed of molecular building blocks chemical versatility and modularity an easy tunability of (opto) electronic properties, structure, crystallinity, and porosity
Thermal properties (thermal conductivity)	3000-5000 W/(m·K)	>300 W/(m·K)	largely reduced due to the presence of periodic holes	13-136 W/(m·K)	promoting: periodic columnar π-arrays and ordered nanochannels; exciton separation and charge transport
Optical properties	optical transmittance (97.7%) from UV and visible to infrared	confined in deep UV range	visible-light-active (up to 460 nm)	from UV to visible, and even NIR region	strong covalent bonds high chemical and thermal stabilities
Electronic properties	zero-band gap On/off ratio (5.5-44) charge carriers mobility of 200,000 $cm^2/(V·S)$ Conduction type (Ambipolar)	indirect band gap (5-6 eV)	band gap (~2.7 eV) the VB position (1.57 eV) the CB position (-1.13 eV)	bandgap from 0.3 eV to 2.0 eV On/off ratio (10000-100000) the hole mobility of 1000 $cm^2/(V·S)$ Conduction type (Ambipolar)	high structural porosity high surface areas rapid diffusion of charges to the surface high interaction surface
Catalytic properties	the large specific surface area of 2630 m^2/g high stability lower calculated Fermi level high charge carriers mobility	a high surface area of 3300 m^2/g high electrical insulation high thermal and chemical stability	its polymeric structure allows for easy modification suitable band potentials for overall water splitting chemical and thermal stability cheap, easily prepared and non-toxic low specific surface area (2-10 m^2/g) insufficient visible light absorption ultrafast recombination electron-hole pairs scarce charge mobility	direct and tunable bandgap extended photon absorption window high carrier mobility unique in-plane anisotropy properties environmental instability	crystallinity and the long-range order facilitating charge transport minimizing charge trapping at defect sites composed of lightweight elements low density high gravimetric performance

Fig. 10. Key photocatalysis-related properties of graphene-like metal-free 2D materials (mechanical, thermal, electrical, optical and catalytic properties of graphene, h-BN, g-C_3N_4 and BP; 6 main aspects of COFs properties). The references have been given in the above review.

(g-C_3N_4), as the most widely studied organic semiconductor material, has elicited intense attention owing to the modest bandgap (~2.70 eV). However, the drawbacks of insufficient visible-light response and fast charge recombination seriously hinder its wide applications. Also, solely composed of triazine or heptazine units, its chemical variations for structural optimization are restricted. Similar to g-C_3N_4, but even more so, COFs are characterized by crystallinity, porosity and tunability, which hold great potential for photocatalysis. Obviously, some properties that have not been found in graphene could be obtained in these nanomaterials.

Revealing the origin of the activity enhancement in turn provides fundamental science to construct photocatalysts based on 2D materials with higher photoactivities. As shown in Fig. 11, we critically summarized recent advances regarding their role in photocatalytic activity enhancement. With selected typical examples, fundamental roles of graphene in graphene-based composite photocatalysts have been found to be diverse. Besides performing as electron transfer mediator and adsorbents, graphene has also been reported the novel photothermal effect and the photosensitizer role recently. BN can transfer or accept electrons as a kind of surface passivation material on one hand and boost the immigration of holes due to electronegative surface on the other. Thanks to the unique electronic structure with both a mild band gap of 2.7 eV

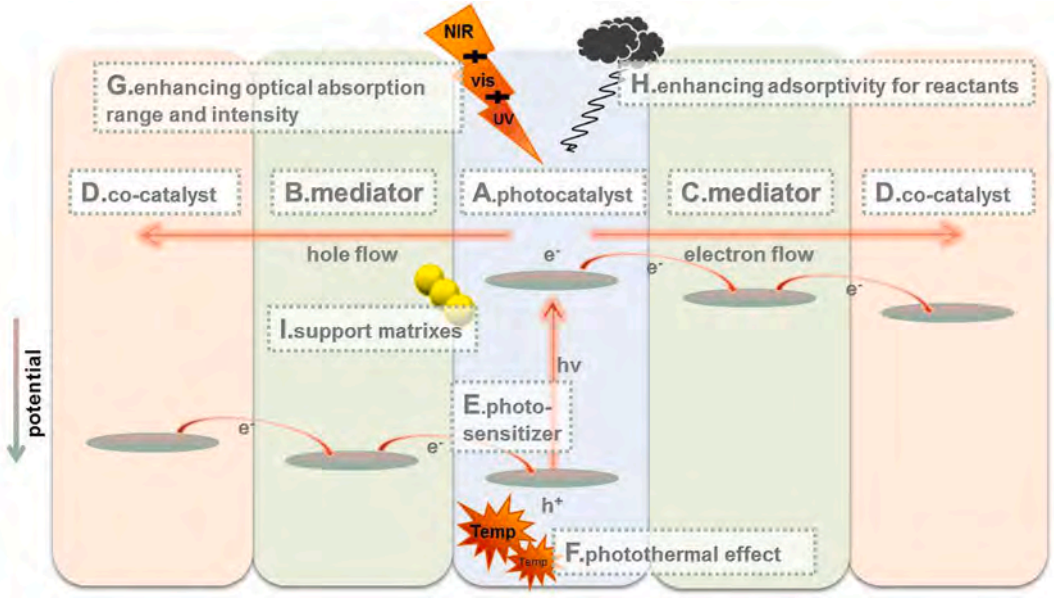

Fig. 11. Schematic illustration of the possible roles of graphene-like metal-free 2D nanomaterials in the activity enhancement of composite photocatalysts.

and appropriate CB and VB positions, g-C_3N_4 itself can serve as a promising visible-light photocatalyst. Moreover, through the reasonable modification measures of g-C_3N_4 including heterojunction construction, nano-structural engineering, element doping, copolymerization and dye sensitization, its photocatalytic applications could be considerably enriched in a more rational manner. So high a hole mobility beyond graphene guarantees it that BP can act as a hole-migration co-catalyst. And standalone BP is also chosen to be a promising visible and NIR-driven photocatalyst. A careful selection of monomers as building blocks will award different types of semiconducting characteristics to COFs. Hence, COFs contain tremendous potential as heterogeneous metal-free semiconductor photocatalyst. Further, its π-conjugated backbones and large surface area perfect the usage as ideal support matrixes.

As considerable progress has been made on GMFs for photocatalysis, more breakthroughs and broad prospects in this burgeoning field are expected. Each graphene-analogous 2D nanomaterial has its own unique strengths and weaknesses that cannot be ignored and should be taken into consideration.

(1) In the case of graphene, the zero-band-gap behavior mainly impedes its semiconducting applications. Besides exploring more strategies to open up a band-gap in graphene, the semiconducting character of its derivatives (GO, rGO) shouldn't be ignored but should be deeply investigated. The detailed roles of graphene in different photocatalytic systems were enumerated in this paper, while it is far from completed. As compared to the role of graphene derivatives as conductive supports, adsorbents and electron transfer acceptors, their photothermal effect and photosensitizer role have been delved less deeply. Moreover, there is a lack of direct experimental evidence to support the photosensitization of graphene. As mentioned before in this review, only when the specific interfacial contact exists between graphene and other component semiconductor can its exact photosensitizer role be observed, so what kind of interface contact will trigger photosensitizer role of graphene? Meanwhile, very little is known about the inherent mechanism of photothermal effect, although photocatalytic activity is enhanced indeed under the phenomenon.
(2) As discussed earlier, every endeavor has been almost made on modifying a semiconductor with BN to optimize their photocatalytic performance, where BN mainly functioned in promoting photogenerated carrier (hole/free electron) transfer and providing large surface areas as adsorption sites. Actually, BN are usually overlooked with regard to its semiconductor properties. The dangling bond like B–O–Ti could be found at the interface of h-BN/TiO_2. Further, BN richly exposed or chemically functionalized by (002) facet edge is highly reactive, and it can also supply active sites for the catalytic reaction. However, this role of BN in photocatalytic fields hasn't been extensively reported.
(3) To achieve a much smoother application of g-C_3N_4 as excellent nonmetallic semiconductor photocatalyst, multiple modifications encompassing adjusting composition, tailoring shape and regulating surface features should be integrated, which are bound up with both thermodynamic and kinetic control. One of the most favorable characteristics of g-C_3N_4 is metal-free nature. We had better choose modification methods like construction of porous structures, dye-sensitization, metal-free doping and metal-free coupling to evade deviating from the initial objective, namely, retaining the metal-free nature. Undoubtedly, cheap, non-toxic and convenient modifications of g-C_3N_4 are preferred to go beyond the lab scale. Furthermore, fine tuning of the interfacial contact between g-C_3N_4 and nanoparticles to control the particle size, hardly gettable, requires various copolymerization strategies to strengthen the anchoring ability of g-C_3N_4.
(4) Despite its auspicious potential as a photocatalyst or co-catalyst, the practical application of black phosphorus (BP) is still facing two thorny issues: (i) No experimental methods to exactly control the layer number of BP. Most of the intrinsic properties of BP are notoriously dependent on the thickness, including its bandgap, the on/off ratio and field effect mobility. A minor deviation of the layer number of BP will evidently affect its performance. Accordingly, development of strategies to adjust the thickness available is imminent. (ii) The innate instability of BP under ambient condition. Exposing the lone pair electrons on the edge, BP is highly reactive to O_2 to form PxOy and would further dissolve in water, leading to its air- and water-instability. Though its hydrophilicity and degradation process under illuminated condition have been studied a lot, the fundamental instability mechanism of BP is hanging in doubt and currently underexplored. Various approaches such as passivation, heterostructure construction, covalent functionalization and aluminum oxide atomic layer deposition (ALD) have been proved to be successful in the protection of BP but may impair its intrinsic properties. Theoretical calculation has reported that heteroatom doping likewise can enhance the life time of BP while no noticeable experimental research has been carried out yet. There is still a huge space to develop reliable and effective protection for maintaining BP quality.
(5) Under harsh conditions, reinforcing the long-term chemical stability of COFs is a platitude but also the most important. The design of COFs with fully sp^2 C═C backbone, leading to fully π-conjugated structure with high chemical stability and optimal electron delocalization in principle, has been one of the key research hotspots recently though challenging. We are expecting that COFs can soon be synthesized successfully by the rational selection of novel organic building blocks and intriguing synthetic methods. Although 2D-COFs are representative of crystalline materials, they are semicrystalline in many cases. Synthesis of COFs with improved crystallinity is still facing big barriers under mild conditions, based on which it's indispensable to understand thoroughly the thermodynamic behavior of dynamic covalent reactions.
(6) Although there are too many uncertainties to accurately calculate the cost, the cost factor studies on solving environmental problems by GMFs-based photocatalysts cannot be ignored. Such cost is driven by three main components: (i) Photocatalysts preparation. To this degree, the price of raw materials, the choice of synthesis methods and the optimization of base conditions should be considered. It is obligated to indicate that the selection of preparation approach should refer to the characteristics of the nanomaterial. (ii) Photocatalysts recyclability. It is of significance for assessing the economy and the use value of photocatalysts. These GMFs-based photocatalysts should be capable of being reused after a lot of water treatment cycles. (iii) Operational conditions. In practical application, the cost spent to the concentration of photocatalysts, to the adjustment of the ambient environment (pH, temperature, etc.) and to the devices (UV lamps, photoreactors, etc.) should be taken into consideration. Accordingly, reducing the uncertainties in cost estimation and developing cost budget models might be of great help to obtain potential cost-effective photocatalytic systems.
(7) When it comes to the roles of 2D materials in the composite photocatalysts based on them, the existing experimental techniques sometimes cannot provide direct evidence to disclose them in-depth and specific enough. Whereas computational modeling can offer tools to simulate the specific microstructures and catalytic reactions at surfaces in parallel with a more scientific elucidation of the experimental phenomena. Theoretical calculation methods such as the ab initio calculation, the Monte Carlo (MC) and molecular dynamics (MD) simulation hold great

potential to illuminate functions of each of these 2D materials parts and the mechanism of interfacial charge transfer in the composite semiconductors. Hence combing the theoretical calculation and experimental technologies should be encouraged in this field. For the same purpose, some state-of-art characterization approaches like operand TEM and transient-state surface photovoltage (SPV) spectroscopy also favor us deepening the understanding on interface coupling between heterojunction components.

Declaration of competing interest

The authors declare that they have no known competing financial interests or personal relationships that could have appeared to influence the work reported in this paper.

Acknowledgements

This work was supported by the Natural Science Foundation of Hunan Province (2019JJ20002), the National Natural Science Foundation of China (51979101, 51679082, 51521006, 51809184), the Hunan Science & Technology Innovation Program (2018RS3037).

Appendix A. Supplementary data

Supplementary data to this article can be found online at https://doi.org/10.1016/j.chemosphere.2021.131254.

References

Adamu, H., Dubey, P., Anderson, J.A., 2016. Probing the role of thermally reduced graphene oxide in enhancing performance of TiO_2 in photocatalytic phenol removal from aqueous environments. Chem. Eng. J. 284, 380–388.
Addamo, M., Bellardita, M., Di Paola, A., Palmisano, L., 2006. Preparation and photoactivity of nanostructured anatase, rutile and brookite TiO_2 thin films. Chem. Commun. 47, 4943–4945.
Ataca, C., Ciraci, S., 2010. Functionalization of BN honeycomb structure by adsorption and substitution of foreign atoms. Phys. Rev. B 82, 165402.
Bai, X., Wang, L., Zhu, Y., 2012. Visible photocatalytic activity enhancement of $ZnWO_4$ by graphene hybridization. ACS Catal. 2, 2769–2778.
Balandin, A.A., Ghosh, S., Bao, W., Calizo, I., Teweldebrhan, D., Miao, F., Lau, C.N., 2008. Superior thermal conductivity of single-layer graphene. Nano Lett. 8, 902–907.
Banerjee, T., Gottschling, K., Savasci, G., Ochsenfeld, C., Lotsch, B.V., 2018. H_2 evolution with covalent organic framework photocatalysts. ACS Energy Lett 3, 400–409.
Banerjee, T., Haase, F., Savasci, G., Gottschling, K., Ochsenfeld, C., Lotsch, B.V., 2017. Single-site photocatalytic H_2 evolution from covalent organic frameworks with molecular cobaloxime co-catalysts. J. Am. Chem. Soc. 139, 16228–16234.
Batmunkh, M., Bat-erdene, M., Shapter, J.G., 2016. Phosphorene and phosphorene-based materials–prospects for future applications. Adv. Mater. 28, 8586–8617.
Bellardita, M., García-lópez, E.I., Marcì, G., Krivtsov, I., García, J.R., Palmisano, L., 2018. Selective photocatalytic oxidation of aromatic alcohols in water by using P-doped g-C_3N_4. Appl. Catal. B Environ. 220, 222–233.
Boukhvalov, D.W., Katsnelson, M.I., 2008. Modeling of graphite oxide. J. Am. Chem. Soc. 130, 10697–10701.
Cassabois, G., Valvin, P., Gil, B., 2016. Hexagonal boron nitride is an indirect bandgap semiconductor. Nat. Photonics 10, 262–266.
Castellanos-gomez, A., 2015. Black phosphorus : narrow gap , wide applications. J. Phys. Chem. Lett. 6, 4280–4291.
Che, H., Che, G., Zhou, P., Liu, C., Dong, H., Li, Chunxue, Song, N., Li, Chunmei, 2020. Nitrogen doped carbon ribbons modified g-C_3N_4 for markedly enhanced photocatalytic H_2-production in visible to near-infrared region. Chem. Eng. J. 382, 122870.
Chen, F., Yang, Q., Wang, Y., Zhao, J., Wang, D., Li, X., Guo, Z., Wang, H., Deng, Y., Niu, C., Zeng, G., 2017a. Novel ternary heterojunction photcocatalyst of Ag nanoparticles and g-C_3N_4 nanosheets co-modified $BiVO_4$ for wider spectrum visible-light photocatalytic degradation of refractory pollutant. Appl. Catal. B Environ. 205, 133–147.
Chen, J., Shi, J., Wang, X., Cui, H., Fu, M., 2013. Recent progress in the preparation and application of semiconductor/graphene composite photocatalysts. Chin. J. Catal. 34, 621–640.
Chen, K., Yang, L., Wu, Z., Chen, C., Jiang, J., Zhang, G., 2019a. A computational study on the tunability of woven covalent organic frameworks for photocatalysis. Phys. Chem. Chem. Phys. 21, 546–553.
Chen, P., Li, N., Chen, X., Ong, W., Zhao, X., 2018a. The rising star of 2D black phosphorus beyond graphene : synthesis , properties and electronic applications. 2D Mater. 5, 014002.
Chen, W., Hua, Y., Wang, Y., Huang, T., Liu, T., Liu, X., 2017b. Two-dimensional mesoporous g-C_3N_4 nanosheet-supported $MgIn_2S_4$ nanoplates as visible-light-active heterostructures for enhanced photocatalytic activity. J. Catal. 349, 8–18.
Chen, X., Li, H., Chen, M., Li, W., Yuan, Z., Snyders, R., 2019b. Visible-light-driven photocatalytic activities of monodisperse ZnS-coated reduced graphene oxide nanocomposites. Mater. Chem. Phys. 227, 368–374.
Chen, Y., Gao, H., Xiang, J., Dong, X., Cao, Y., 2018b. Enhanced photocatalytic activities of TiO_2-reduced graphene oxide nanocomposites controlled by Ti–O–C interfacial chemical bond. Mater. Res. Bull. 99, 29–36.
Chen, Z., Chen, X., Di, J., Liu, Y., Yin, S., Xia, J., Li, H., 2017c. Graphene-like boron nitride modified bismuth phosphate materials for boosting photocatalytic degradation of enrofloxacin. J. Colloid Interface Sci. 492, 51–60.
Co, A.P., Benin, A.I., Ockwig, N.W., Keeffe, M.O., Matzger, A.J., Yaghi, O.M., 2005. Porous, crystalline, covalent organic frameworks. Science 310, 1166–1170.
Dalapati, S., Addicoat, M., Jin, S., Sakurai, T., Gao, J., Xu, H., Irle, S., Seki, S., Jiang, D., 2015. Rational design of crystalline supermicroporous covalent organic frameworks with triangular topologies. Nat. Commun. 6, 1–8.
Di, J., Xia, J., Ji, M., Wang, B., Yin, S., Zhang, Q., Chen, Z., Li, H., 2016. Environmental advanced photocatalytic performance of graphene-like BN modified BiOBr flower-like materials for the removal of pollutants and mechanism insight. Appl. Catal. B Environ. 183, 254–262.
Ding, J., Xu, W., Wan, H., Yuan, D., Chen, C., Wang, L., Guan, G., Dai, W.-L., 2018. Nitrogen vacancy engineered graphitic C_3N_4-based polymers for photocatalytic oxidation of aromatic alcohols to aldehydes. Appl. Catal. B Environ. 221, 626–634.
Ding, X., Guo, Jia, Feng, X., Honsho, Y., Guo, Jingdong, Seki, S., Maitarad, P., Saeki, A., Nagase, S., Jiang, D., 2011. Synthesis of metallophthalocyanine covalent organic frameworks that exhibit high carrier mobility and photoconductivity. Angew. Chem. Int. Ed. 50, 1289–1293.
Dong, F., Li, Y., Wang, Z., Ho, W., 2015. Enhanced visible light photocatalytic activity and oxidation ability of porous graphene-like g-C_3N_4 nanosheets via thermal exfoliation. Appl. Surf. Sci. 358, 393–403.
Dong, X., Cheng, F., 2015. Recent development in exfoliated two-dimensional g-C_3N_4 nanosheets for photocatalytic applications. J. Mater. Chem. 3, 23642–23652.
Du, A., Ng, Y.H., Bell, N.J., Zhu, Z., Amal, R., Smith, S.C., 2011. Hybrid graphene/titania nanocomposite: interface charge transfer, hole doping, and sensitization for visible light response. J. Phys. Chem. Lett. 2, 894–899.
Du, A., Sanvito, S., Li, Z., Wang, D., Jiao, Y., Liao, T., Sun, Q., Ng, Y.H., Zhu, Z., Amal, R., Smith, S.C., 2012. Hybrid graphene and graphitic carbon nitride nanocomposite: gap opening, electron – hole puddle, interfacial charge transfer, and enhanced visible light response. J. Am. Chem. Soc. 134, 4393–4397.
Finegold, L., Cude, J.L., 1972. One and two-dimensional structure of alpha-helix and beta-sheet forms of poly (L-Alanine) shown by specific heat measurements at low temperatures (1.5-20 K). Nature 238, 38–40.
Fu, Q., Bao, X., 2017. Surface chemistry and catalysis confined under two-dimensional materials. Chem. Soc. Rev. 46, 1842–1874.
Fu, X., Hu, Y., Yang, Y., Liu, W., Chen, S., 2013a. Ball milled h-BN : an efficient holes transfer promoter to enhance the photocatalytic performance of TiO_2. J. Hazard Mater. 244–245, 102–110.
Fu, X., Hu, Y., Zhang, T., Chen, S., 2013b. The role of ball milled h-BN in the enhanced photocatalytic activity : a study based on the model of ZnO. Appl. Surf. Sci. 280, 828–835.
Gan, Z., Wu, X., Meng, M., Zhu, X., Yang, L., Chu, P.K., 2014. Photothermal contribution to enhanced photocatalytic performance of graphene-based nanocomposites. ACS Nano 8, 9304–9310.
Gao, E., Wang, W., Shang, M., Xu, J., 2011. Synthesis and enhanced photocatalytic performance of graphene-Bi_2WO_6 composite. Chem. Chem. Phys. 13, 2887–2893.
Geim, A.K., Grigorieva, I.V., 2013. Van der Waals heterostructures. Nature 499, 419–425.
Godin, R., Wang, Y., Zwijnenburg, M.A., Tang, J., Durrant, J.R., 2017. Time-resolved spectroscopic investigation of charge trapping in carbon nitrides photocatalysts for hydrogen generation. J. Am. Chem. Soc. 139, 5216–5224.
Golberg, D., Bando, Y., Huang, Y., Terao, T., Mitome, M., Tang, C., Zhi, C., 2010. Boron nitride nanotubes and nanosheets. ACS Nano 4, 2979–2993.
Gu, J., Yan, J., Chen, Z., Ji, H., Song, Y., Fan, Y., Xu, H., Li, H., 2017. Construction and preparation of novel 2D metal-free few-layer BN modified graphene-like g-C_3N_4 with enhanced photocatalytic performance. Dalton Trans. 46, 11250–11258.
Guo, J., Jiang, L., Liang, J., Xu, W., Yu, H., Zhang, J., Ye, S., Xing, W., Yuan, X., 2021a. Photocatalytic degradation of tetracycline antibiotics using delafossite silver ferrite-based Z-scheme photocatalyst: pathways and mechanism insight. Chemosphere 270, 128651.
Guo, J., Li, X., Liang, J., Yuan, X., Jiang, L., Yu, H., Sun, H., Zhu, Z., Ye, S., Tang, N., Zhang, J., 2021b. Fabrication and regulation of vacancy-mediated bismuth oxyhalide towards photocatalytic application: development status and tendency. Coord. Chem. Rev. 443, 214033.
Guo, J., Liang, J., Yuan, X., Jiang, L., Zeng, G., Yu, H., Zhang, J., 2018. Efficient visible-light driven photocatalyst, silver (meta)vanadate: synthesis, morphology and modification. Chem. Eng. J. 352, 782–802.
Gustavsson, L., Haus, S., Lundblad, M., Lundström, A., Ortiz, C.A., Sathre, R., Truong, N. Le, Wikberg, P.E., 2017. Climate change effects of forestry and substitution of carbon-intensive materials and fossil fuels. Renew. Sustain. Energy Rev. 67, 612–624.
Han, Q., Wang, B., Zhao, Y., Hu, C., Qu, L., 2015. A Graphitic-C_3N_4 "seaweed" architecture for enhanced hydrogen evolution. Angew. Chem. Int. Ed. 54, 11433–11437.
He, S., Rong, Q., Niu, H., Cai, Y., 2017. Construction of a superior visible-light-driven photocatalyst based on a C_3N_4 active centre-photoelectron shift platform-electron

withdrawing unit triadic structure covalent organic framework. Chem. Commun. 53, 9636–9639.
Hoffmann, M.R., Martin, S.T., Choi, W., Bahnemann, D.W., 1995. Environmental applications of semiconductor photocatalysis. Chem. Rev. 95, 69–96.
Hong, Y., Jiang, Y., Li, C., Fan, W., Yan, X., Yan, M., Shi, W., 2016. In-situ synthesis of direct solid-state Z-scheme V_2O_5/g-C_3N_4 heterojunctions with enhanced visible light efficiency in photocatalytic degradation of pollutants. Appl. Catal. B Environ. 180, 663–673.
Hu, C., Lin, Y., Connell, J.W., Cheng, H.-M., Gogotsi, Y., Titirici, M.-M., Dai, L., 2019. Carbon-based metal-free catalysts for energy storage and environmental remediation. Adv. Mater. 31, 1806128.
Hu, Z.T., Liu, J., Yan, X., Oh, W. Da, Lim, T.T., 2015. Low-temperature synthesis of graphene/$Bi_2Fe_4O_9$ composite for synergistic adsorption-photocatalytic degradation of hydrophobic pollutant under solar irradiation. Chem. Eng. J. 262, 1022–1032.
Huang, H., Xiao, K., Tian, N., Dong, F., Zhang, T., Du, X., Zhang, Y., 2017. Template-free precursor-surface-etching route to porous, thin g-C_3N_4 nanosheets for enhancing photocatalytic reduction and oxidation activity. J. Mater. Chem. 5, 17452–17463.
Huang, W., Ma, B.C., Lu, H., Li, R., Wang, L., Landfester, K., Zhang, K.A.I., 2017. Visible-light-promoted selective oxidation of alcohols using a covalent triazine framework. ACS Catal. 7, 5438–5442.
Hultgren, R., Gingrich, N.S., Warren, B.E., 1935. The atomic distribution in red and black phosphorus and the crystal structure of black phosphorus. J. Chem. Phys. 3, 351–355.
Jain, R., Narayan, R., Sasikala, S.P., Lee, K.E., Jung, H.J., Kim, S.O., 2017. Phosphorene for energy and catalytic application — filling the gap between graphene and 2D metal chalcogenides. 2D Mater. 4, 042006.
Jang, H., Wood, J.D., Ryder, C.R., Hersam, M.C., Cahill, D.G., 2015. Anisotropic thermal conductivity of exfoliated black phosphorus. Adv. Mater. 27, 8017–8022.
Ji, M., Xia, J., Di, J., Liu, Y., Chen, R., Chen, Z., Yin, S., L, H., 2018. Graphene-like boron nitride induced accelerated charge transfer for boosting the photocatalytic behavior of $Bi_4O_5I_2$ towards bisphenol a removal. Chem. Eng. J. 331, 355–363.
Jiang, L., Yuan, X., Pan, Y., Liang, J., Zeng, G., Wu, Z., Wang, H., 2017a. Doping of graphitic carbon nitride for photocatalysis : a reveiw. Appl. Catal. B Environ. 217, 388–406.
Jiang, L., Yuan, X., Zeng, G., Chen, X., Wu, Z., Liang, J., Zhang, J., Wang, Hui, Wang, Hou, 2017b. Phosphorus- and sulfur-codoped g-C_3N_4 : facile preparation, mechanism insight, and application as efficient photocatalyst for tetracycline and methyl orange degradation under visible light irradiation. ACS Sustain. Chem. Eng. 5, 5831–5841.
Jiang, L., Yuan, X., Zeng, G., Liang, J., Chen, X., Yu, H., Wang, H., Wu, Z., Zhang, J., Xiong, T., 2018a. In-situ synthesis of direct solid-state dual Z-scheme WO_3/g-C_3N_4/Bi_2O_3 photocatalyst for the degradation of refractory pollutant. Appl. Catal. B Environ. 227, 376–385.
Jiang, L., Yuan, X., Zeng, G., Liang, J., Wu, Z., Wang, H., 2018b. Environmental science nano construction of an all-solid-state Z-scheme and its enhancement to catalytic activity. Environ.Sci. Nano 5, 599–615.
Jiang, L., Yuan, X., Zeng, G., Liang, J., Wu, Z., Wang, H., Zhang, J., Xiong, T., Li, H., 2018c. A facile band alignment of polymeric carbon nitride isotype heterojunctions for enhanced photocatalytic tetracycline degradation. Environ. Sci. Nano 5, 2604–2617.
Jiang, L., Yuan, X., Zeng, G., Liang, J., Wu, Z., Yu, H., Mo, D., Wang, H., Xiao, Z., Zhou, C., 2019. Nitrogen self-doped g-C_3N_4 nanosheets with tunable band structures for enhanced photocatalytic tetracycline degradation. J. Colloid Interface Sci. 536, 17–29.
Jiang, L., Yuan, X., Zeng, G., Wu, Z., Liang, J., Chen, X., Leng, L., Wang, Hui, Wang, Hou, 2018d. Metal-free efficient photocatalyst for stable visible-light photocatalytic degradation of refractory pollutant. Appl. Catal. B Environ. 221, 715–725.
Jiang, W., Bai, S., Wang, L., Wang, X., Yang, L., Li, Y., Liu, D., 2016. Integration of multiple plasmonic and co-catalyst nanostructures on TiO_2 nanosheets for visible-near- infrared photocatalytic hydrogen evolution. Small 12, 1640–1648.
Jilani, A., Othman, M.H.D., Ansari, M.O., Hussain, S.Z., Ismail, A.F., Khan, I.U., Inamuddin, 2018. Graphene and its derivatives: synthesis, modifications, and applications in wastewater treatment. Environ. Chem. Lett. 16, 1301–1323.
Jin, K.H., Choi, S.M., Jhi, S.H., 2010. Crossover in the adsorption properties of alkali metals on graphene. Phys. Rev. B 82, 033414.
Karim, M.R., Rahman, M.M., Asiri, A.M., Hayami, S., 2020. Branched alkylamine-reduced graphene oxide hybrids as a dual proton-electron conductor and organic-only water-splitting photocatalyst. ACS Appl. Mater. Interfaces 12, 10829–10838.
Kiran, B., Manga, K., Zhou, Y., Yan, Y., Loh, K.P., 2009. Multilayer hybrid films consisting of alternating graphene and titania nanosheets with ultrafast electron transfer and photoconversion properties. Adv. Funct. Mater. 19, 3638–3643.
Kouser, S., Thannikoth, A., Gupta, U., Waghmare, U.V., Rao, C.N.R., 2015. 2D-GaS as a photocatalyst for water splitting to produce H_2. Small 11, 4723–4730.
Kuhn, P., Antonietti, M., Thomas, A., 2008. Porous , Covalent triazine-based frameworks prepared by ionothermal synthesis. Angew. Chem. Int. Ed. 47, 3450–3453.
Lang, Q., Chen, Y., Huang, T., Yang, L., Zhong, S., Wu, L., Chen, J., Bai, S., 2018. Graphene "bridge" in transferring hot electrons from plasmonic Ag nanocubes to TiO_2 nanosheets for enhanced visible light photocatalytic hydrogen evolution. Appl. Catal. B Environ. 220, 182–190.
Lee, C., Wei, X., Kysar, J.W., Hone, J., 2008. Measurement of the elastic properties and intrinsic strength of monolayer graphene. Science 321, 385–388.
Lee, E., Hong, J.Y., Kang, H., Jang, J., 2012. Synthesis of TiO_2 nanorod-decorated graphene sheets and their highly efficient photocatalytic activities under visible-light irradiation. J. Hazard Mater. 219–220, 13–18.
Lee, J.S., You, K.H., Park, C.B., 2012. Highly photoactive, low bandgap TiO_2 nanoparticles wrapped by graphene. Adv. Mater. 24, 1084–1088.
Lewis, N.S., Nocera, D.G., 2006. Powering the planet: chemical challenges in solar energy utilization. Proc. Natl. Acad. Sci. U.S.A. 103, 15729–15735.
Li, B., Lai, C., Zeng, G., Huang, D., Qin, L., Zhang, M., Cheng, M., Liu, X., Yi, H., Zhou, C., Huang, F., Liu, S., Fu, Y., 2019. Black Phosphorus, a rising star 2D nanomaterial in the post-graphene era: synthesis, properties, modifications, and photocatalysis applications. Small 15, 1–30, 1804565.
Li, H., Hu, H., Bao, C., Guo, F., Zhang, X., Liu, Xiaobiao, Hua, J., Tan, J., Wang, A., Zhou, H., Yang, B., Qu, Y., Liu, Xiangdong, 2016. Forming heterojunction: an effective strategy to enhance the photocatalytic efficiency of a new metal-free organic photocatalyst for water splitting. Sci. Rep. 6, 1–10.
Li, J., Xing, Q., Zhou, Y., Huang, H., Dong, F., 2018. The activation of reactants and intermediates promotes the selective photocatalytic NO conversion on electron-localized Sr-intercalated g-C_3N_4. Appl. Catal. B Environ. 232, 69–76.
Li, L., Yu, Y., Ye, G.J., Ge, Q., Ou, X., Wu, H., Feng, D., Chen, X.H., Zhang, Y., 2014. Black phosphorus field-effect transistors. Nat. Nanotechnol. 9, 372–377.
Li, M., Wang, Y., Tang, P., Xie, N., Zhao, Yunxuan, Liu, X., Hu, G., Xie, J., Zhao, Yufei, Tang, J., Zhang, T., 2017. Graphene with atomic-level in-plane decoration of h-BN domains for efficient photocatalysis. Chem. Mater. 29, 2769–2776.
Li, S., Chen, J., Hu, S., Wang, H., Jiang, W., Chen, X., 2020. Facile construction of novel Bi_2WO_6/Ta_3N_5 Z-scheme heterojunction nanofibers for efficient degradation of harmful pharmaceutical pollutants. Chem. Eng. J. 402, 126165.
Li, X., Zhang, C., Cai, S., Lei, X., Altoe, V., Hong, F., Urban, J.J., Ciston, J., Chan, E.M., Liu, Y., 2018. Facile transformation of imine covalent organic frameworks into ultrastable crystalline porous aromatic frameworks. Nat. Commun. 9, 2998.
Li, Yibing, Zhang, H., Liu, P., Wang, D., Li, Ying, Zhao, H., 2013. Cross-linked g-C_3N_4/rGO nanocomposites with tunable band structure and enhanced visible light photocatalytic activity. Small 9, 3336–3344.
Liu, B., Zhou, K., 2019. Recent progress on graphene-analogous 2D nanomaterials : properties , modeling and applications. Prog. Mater. Sci. 100, 99–169.
Liu, C., Zhang, Y., Dong, F., Reshak, A.H., Ye, L., Pinna, N., Zeng, C., Zhang, T., Huang, H., 2017. Chlorine intercalation in graphitic carbon nitride for efficient photocatalysis. Appl. Catal. B Environ. 203, 465–474.
Liu, H., Chen, D., Wang, Z., Jing, H., Zhang, R., 2017. Microwave-assisted molten-salt rapid synthesis of isotype triazine-/heptazine based g-C_3N_4 heterojunctions with highly enhanced photocatalytic hydrogen evolution performance. Appl. Catal. B Environ. 203, 300–313.
Liu, H., Neal, A.T., Zhu, Z., Luo, Z., Xu, X., Nek, D.T., Ye, P.D., 2014. Phosphorene : an unexplored 2D semiconductor with a high hole mobility. ACS Nano 8, 4033–4041.
Liu, J., 2015. Origin of high photocatalytic efficiency in monolayer g-C3N4/CdS heterostructure: a hybrid DFT study. J. Phys. Chem. C 119, 28417–28423.
Liu, J., Yu, Y., Qi, R., Cao, C., Liu, X., Zheng, Y., Song, W., 2019. Enhanced electron separation on in-plane benzene-ring doped g-C_3N_4 nanosheets for visible light photocatalytic hydrogen evolution. Appl. Catal. B Environ. 244, 459–464.
Loh, K.P., Bao, Q., Ang, P.K., Yang, J., 2010. The chemistry of graphene. J. Mater. Chem. 20, 2277–2289.
Low, J., Cao, S., Yu, J., Wageh, S., 2014. Two-dimensional layered composite photocatalysts. Chem. Commun. 50, 10768–10777.
Luo, M., Yang, Q., Liu, K., Cao, H., Yan, H., 2019. Boosting photocatalytic H_2 evolution on g-C_3N_4 by modifying covalent organic frameworks (COFs). Chem. Commun. 55, 5829–5832.
Lv, X., Wang, J., Yan, Z., Jiang, D., Liu, J., 2016. Design of 3D h- BN architecture as Ag_3VO_4 enhanced photocatalysis stabilizer and promoter. J. Mol. Catal. Chem. 418–419, 146–153.
Mahmoudi, T., Wang, Y., Hahn, Y.B., 2019. $SrTiO_3$/Al_2O_3-graphene electron transport layer for highly stable and efficient composites-based perovskite solar cells with 20.6% efficiency. Adv. Energy Mater. 10, 1903369.
Meng, J., Wang, X., Liu, Y., Ren, M., Zhang, X., Ding, X., Guo, Y., Yang, Y., 2021. Acid-induced molecule self-assembly synthesis of Z-scheme WO_3/g-C_3N_4 heterojunctions for robust photocatalysis against phenolic pollutants. Chem. Eng. J. 403, 126354.
Meng, S., Ye, X., Ning, X., Xie, M., Fu, X., Chen, S., 2016. Selective oxidation of aromatic alcohols to aromatic aldehydes by BN/metal sulfide with enhanced photocatalytic activity. Appl. Catal. B Environ. 182, 356–368.
Nair, R.R., Blake, P., Novoselov, K.S., Booth, T.J., Stauber, T., Peres, N.M.R., Geim, A.K., 2008. Fine structure constant defines visual transparency of graphene. Science 320, 1308.
Natarajan, S., Bajaj, H.C., 2016. Recovered materials from spent lithium-ion batteries (LIBs) as adsorbents for dye removal: equilibrium, kinetics and mechanism. J. Environ. Chem. Eng. 4, 4631–4643.
Neelgund, G.M., Bliznyuk, V.N., Oki, A., 2016. Photocatalytic activity and NIR laser response of polyaniline conjugated graphene nanocomposite prepared by a novel acid-less method. Appl. Catal. B Environ. 187, 357–366.
Niu, P., Zhang, L., Liu, G., Cheng, H., 2012. Graphene-like carbon nitride nanosheets for improved photocatalytic activities. Adv. Funct. Mater. 22, 4763–4770.
Novoselov, K.S., Geim, A.K., Morozov, S.V., Jiang, D., Zhang, Y., V, D.S., Grigorieva, I.V. A.F.A., 2004. Electric field effect in atomically thin carbon films. Science 306, 666–669.
Novoselov, K.S., Mishchenko, A., Carvalho, A., Neto, A.H.C., 2016. 2D materials and van der Waals heterostructures. Science 353, 6298.
Ong, W.J., Tan, L.L., Chai, S.P., Yong, S.T., 2015a. Graphene oxide as a structure-directing agent for the two-dimensional interface engineering of sandwich-like graphene-g-C_3N_4 hybrid nanostructures with enhanced visible-light photoreduction of CO_2 to methane. Chem. Commun. 51, 858–861.
Ong, W.J., Tan, L.L., Chai, S.P., Yong, S.T., Mohamed, A.R., 2015b. Surface charge modification via protonation of graphitic carbon nitride (g-C_3N_4) for electrostatic self-assembly construction of 2D/2D reduced graphene oxide (rGO)/g-C_3N_4

nanostructures toward enhanced photocatalytic reduction of carbon dioxide to methane. Nanomater. Energy 13, 757–770.
Orooji, Y., Ghanbari, M., Amiri, O., Salavati-Niasari, M., 2020. Facile fabrication of silver iodide/graphitic carbon nitride nanocomposites by notable photo-catalytic performance through sunlight and antimicrobial activity. J. Hazard Mater. 389, 122079.
Patnaik, S., Sahoo, D.P., Parida, K., 2018. An overview on Ag modified g-C_3N_4 based nanostructured materials for energy and environmental applications. Renew. Sustain. Energy Rev. 82, 1297–1312.
Peng, Y., Zhao, M., Chen, B., Zhang, Z., Huang, Y., Dai, F., Lai, Z., Cui, X., Tan, C., Zhang, H., 2018. Hybridization of MOFs and COFs: a new strategy for construction of MOF@COF core–shell hybrid materials. Adv. Mater. 30 (1–5), 1705454.
Qin, J., Huo, J., Zhang, P., Zeng, J., Wang, T., Zeng, H., 2016. Improving the photocatalytic hydrogen production of Ag/g-C_3N_4 nanocomposites by dye-sensitization under visible light irradiation. Nanoscale 8, 2249–2259.
Rahman, M.Z., Kibria, M.G., Mullins, Charles Buddie, 2020. Metal-free photocatalysts for hydrogen evolution. Chem. Soc. Rev. 49, 1887–1931.
Ran, J., Guo, W., Wang, H., Zhu, B., Yu, J., Qiao, S., 2018. Metal-free 2D/2D phosphorene/g-C_3N_4 van der waals heterojunction for highly enhanced visible-light photocatalytic H_2 production. Adv. Mater. 30, 1800128.
Ran, J., Zhu, B., Qiao, S., 2017. Phosphorene co-catalyst advancing highly efficient visible-light photocatalytic hydrogen production. Angew. Chem. Int. Ed. 56, 10373–10377.
Ranjith, K.S., Manivel, P., Rajendrakumar, R.T., Uyar, T., 2017. Multifunctional ZnO nanorod-reduced graphene oxide hybrids nanocomposites for effective water remediation: effective sunlight driven degradation of organic dyes and rapid heavy metal adsorption. Chem. Eng. J. 325, 588–600.
Robinson, J.T., Tabakman, S.M., Liang, Y., Wang, H., Casalongue, H.S., Vinh, D., Dai, H., 2011. Ultrasmall reduced graphene oxide with high near-infrared absorbance for photothermal therapy. J. Am. Chem. Soc. 133, 6825–6831.
Ruzicka, B.A., Werake, L.K., Zhao, H., Wang, S., Loh, K.P., 2010. Femtosecond pump-probe studies of reduced graphene oxide thin films. Appl. Phys. Lett. 96, 173106.
Schwarz, D., Acharjya, A., Ichangi, A., Kochergin, Y.S., Lyu, P., Opanasenko, M.V., Tarábek, J., Chocholousová, J.V., Vacek, J., Schmidt, J., Cejka, J., Nachtigall, P., Thomas, A., Bojdys, M.J., 2019. Tuning the porosity and photocatalytic performance of triazine-based graphdiyne polymers through polymorphism. ChemSusChem 12, 194–199.
Serrà, A., Zhang, Y., Sepúlveda, B., Gómez, E., Nogués, J., Michler, J., Philippe, L., 2020. Highly reduced ecotoxicity of ZnO-based micro/nanostructures on aquatic biota: influence of architecture, chemical composition, fixation, and photocatalytic efficiency. Water Res. 169, 115210.
Shanmugam, M., Jacobs-gedrim, R., Durcan, C., Yu, B., 2013. 2D layered insulator hexagonal boron nitride enabled surface passivation in dye sensitized solar cells. Nanoscale 5, 11275–11282.
She, X., Liu, L., Ji, H., Mo, Z., Li, Y., Huang, L., Du, D., Xu, H., Li, H., 2016. Environmental Template-free synthesis of 2D porous ultrathin nonmetal-doped g-C_3N_4 nanosheets with highly efficient photocatalytic H_2 evolution from water under visible light. Appl. Catal. B Environ. 187, 144–153.
Sheng, Y., Yang, J., Wang, F., Liu, L., Liu, H., Yan, C., Guo, Z., 2019. Sol-gel synthesized hexagonal boron nitride/titania nanocomposites with enhanced photocatalytic activity. Appl. Surf. Sci. 465, 154–163.
Shi, L., Liang, L., Wang, F., Sun, J., 2014. Polycondensation of guanidine hydrochloride into a graphitic carbon nitride semiconductor with a large surface area as a visible light photocatalyst. Catal. Sci. Technol. 4, 3235–3243.
Si, Y., Xia, Y., Shang, S., Xiong, X., Zeng, X., Zhou, J., Li, Y., 2018. Enhanced visible light driven photocatalytic behavior of BiFeO3/reduced graphene oxide composites. Nanomaterials 8, 526.
Sick, T., Hufnagel, A.G., Kampmann, J., Kondofersky, I., Calik, M., Rotter, J.M., Evans, A., Do, M., Herbert, S., Peters, K., Bo, D., Knochel, P., Medina, D.D., Fattakhova-rohl, D., Bein, T., 2018. Oriented films of conjugated 2D covalent organic frameworks as photocathodes for water splitting. J. Am. Chem. Soc. 140, 2085–2092.
Singh, J., Rishikesh Kumar, S., Soni, R.K., 2020. Synthesis of 3D-MoS_2 nanoflowers with tunable surface area for the application in photocatalysis and SERS based sensing. J. Alloys Compd. 849, 156502.
Song, L., Liu, Z., Leela, A., Reddy, M., Narayanan, N.T., Taha-tijerina, J., Peng, J., Gao, G., Lou, J., Vajtai, R., Ajayan, P.M., 2012. Binary and ternary atomic layers built from carbon , boron , and nitrogen. Adv. Mater. 24, 4878–4895.
Stegbauer, L., Schwinghammer, K., Lotsch, B.V., 2014. A hydrazone-based covalent organic framework for photocatalytic hydrogen production. Chem. Sci. 5, 2789–2793.
Stegbauer, L., Zech, S., Savasci, G., Banerjee, T., Podjaski, F., Schwinghammer, K., Ochsenfeld, C., Lotsch, B.V., 2018. Tailor-made photoconductive pyrene-based covalent organic frameworks for visible-light driven hydrogen generation. Adv. Energy Mater. 8 (1–8), 1703278.
Stoller, M.D., Park, S., Zhu, Y., An, J., Ruoff, R.S., 2008. Graphene-based ultracapacitors. Nano Lett. 8, 3498–3502.
Sun, L., Du, T., Hu, C., Chen, J., Lu, J., Lu, Z., Han, H., 2017. Antibacterial activity of graphene oxide/g-C_3N_4 composite through photocatalytic disinfection under visible light. ACS Sustain. Chem. Eng. 5, 8693–8701.
Sun, Y., Gao, S., Lei, F., Xie, Y., 2015. Atomically-thin two-dimensional sheets for understanding active sites in catalysis. Chem. Soc. Rev. 44, 623–636.
Thomas, A., Fischer, A., Goettmann, F., Antonietti, M., Mu, J., Schlögl, R., Carlsson, J.M., 2008. Graphitic carbon nitride materials: variation of structure and morphology and their use as metal-free catalysts. J. Mater. Chem. 18, 4893–4908.
Thote, J., Aiyappa, H.B., Deshpande, A., Díaz Díaz, D., Kurungot, S., Banerjee, R., 2014. A covalent organic framework-cadmium sulfide hybrid as a prototype photocatalyst for visible-light-driven hydrogen production. Chem. Eur J. 20, 15961–15965.
Tong, Z., Yang, D., Li, Z., Nan, Y., Ding, F., Shen, Y., Jiang, Z., 2017. Thylakoid-inspired multishell g-C_3N_4 nanocapsules with enhanced visible-light harvesting and electron transfer properties for high-efficiency photocatalysis. ACS Nano 11, 1103–1112.
Tong, Z., Yang, D., Sun, Y., Nan, Y., Jiang, Z., 2016. Tubular g-C_3N_4 isotype heterojunction : enhanced visible-light photocatalytic activity through cooperative manipulation of oriented electron and hole transfer. Small 12, 4093–4101.
Tran, V., Soklaski, R., Liang, Y., Yang, L., 2014. Layer-controlled band gap and anisotropic excitons in few-layer black phosphorus. Phys. Rev. B 89, 235319.
Upadhyay, R.K., Soin, N., Roy, S.S., 2014. Role of graphene/metal oxide composites as photocatalysts, adsorbents and disinfectants in water treatment: a review. RSC Adv. 4, 3823–3851.
Vyas, V.S., Haase, F., Stegbauer, L., Savasci, G., Podjaski, F., Ochsenfeld, C., Lotsch, B.V., 2015. A tunable azine covalent organic framework platform for visible light-induced hydrogen generation. Nat. Commun. 6, 1–9.
Wang, C., Chen, R., Shi, J.-L., Ma, Y., Lin, G., Lang, X., 2019. Designed synthesis of a 2D porphyrin-based sp^2 carbon-conjugated covalent organic framework for heterogeneous photocatalysis. Angew. Chem. Int. Ed. 58, 6430–6434.
Wang, H., Zhang, X., Xie, Y., 2018. Photocatalysis in two-dimensional black phosphorus: the roles of many-body effects. ACS Nano 12, 9648–9653.
Weng, Q., Ide, Y., Wang, Xuebin, Wang, Xi, Zhang, C., Jiang, X., Xue, Y., Dai, P., Komaguchi, K., Bando, Y., Golberg, D., 2015. Design of BN porous sheets with richly exposed (002) plane edges and their application as TiO_2 visible light sensitizer. Nanomater. Energy 16, 19–27.
Wu, Q., Liu, Y., Jing, H., Yu, H., Lu, Y., Huo, M., Huo, H., 2020. Peculiar synergetic effect of γ-Fe_2O_3 nanoparticles and graphene oxide on MIL-53 (Fe) for boosting photocatalysis. Chem. Eng. J. 390, 124615.
Wu, X., Ma, H., Zhong, W., Fan, J., Yu, H., 2020. Porous crystalline g-C_3N_4: bifunctional $NaHCO_3$ template-mediated synthesis and improved photocatalytic H_2-evolution rate. Appl. Catal. B Environ. 271, 118899.
Wu, Y., Wang, H., Tu, W., Wu, S., Liu, Y., Tan, Y.Z., Luo, H., Yuan, X., Chew, J.W., 2018. Petal-like CdS nanostructures coated with exfoliated sulfur-doped carbon nitride via chemically activated chain termination for enhanced visible-light–driven photocatalytic water purification and H_2 generation. Appl. Catal. B Environ. 229, 181–191.
Xiong, T., Cen, W., Zhang, Y., Dong, F., 2016. Bridging the g-C_3N_4 interlayers for enhanced photocatalysis. ACS Catal. 6, 2462–2472.
Xu, H., Liu, L., Song, Y., Huang, L., Li, Y., Chen, Z., Zhang, Q., Li, H., 2016. BN nanosheets modi filed WO_3 photocatalysts for enhancing photocatalytic properties under visible light irradiation. J. Alloys Compd. 660, 48–54.
Xu, H., Wu, Z., Ding, M., Gao, X., 2017. Microwave-assisted synthesis of flower-like BN/BiOCl composites for photocatalytic Cr (VI) reduction upon visible-light irradiation. Mater. Des. 114, 129–138.
Xue, C., Yan, X., An, H., Li, H., Wei, J., Yang, G., 2018. Bonding CdS-Sn_2S_3 eutectic clusters on graphene nanosheets with unusually photoreaction-driven structural reconfiguration effect for excellent H_2 evolution and Cr(VI) reduction. Appl. Catal. B Environ. 222, 157–166.
Yan, J., Gu, J., Wang, X., Fan, Y., Zhao, Y., Lian, J., Xu, Y., Song, Y., Xu, H., Li, H., 2017. Design of 3D WO_3/h-BN nanocomposites for efficient visible-light-driven photocatalysis. RSC Adv. 7, 25160–25170.
Yang, L., Wei, D., 2016. Semiconducting covalent organic frameworks : a type of two-dimensional conducting polymers. Chin. Chem. Lett. 27, 1395–1404.
Yang, M.-Q., Zhang, N., Pagliaro, M., Xu, Y.-J., 2014. Artificial photosynthesis over graphene– semiconductor composites. Are we getting better? Chem. Soc. Rev. 43, 8240–8254.
Yang, M., Xu, Y., 2013. Basic principles for observing the photosensitizer role of graphene in the graphene− semiconductor composite photocatalyst from a case study on graphene−zno. J. Phys. Chem. C 117, 21724–21734.
Yang, Q., Luo, M., Liu, K., Cao, H., Yan, H., 2020. Environmental covalent organic frameworks for photocatalytic applications. Appl. Catal. B Environ. 276, 119174.
Yang, S., Hu, W., Zhang, Xin, He, P., Pattengale, B., Liu, C., Cendejas, M., Hermans, I., Zhang, Xiaoyi, Zhang, J., Huang, J., 2018. 2D covalent organic frameworks as intrinsic photocatalysts for visible light-driven CO_2 reduction. J. Am. Chem. Soc. 140, 14614–14618.
Yang, W., Zhang, X., Xie, Y., 2016. Advances and challenges in chemistry of two-dimensional nanosheets. Nano Today 11, 793–816.
Yang, Y., Yin, H., Li, Huifan, Zou, Q., Zhang, Z., Pei, W., Luo, L., Huo, Y., Li, Hexing, 2018. Synergistic photocatalytic-photothermal contribution to antibacterial activity in BiOI-graphene oxide nanocomposites. ACS Appl. Bio Mater. 1, 2141–2152.
Yeh, B.T., Syu, J., Cheng, C., Chang, T., Teng, H., 2010. Graphite oxide as a photocatalyst for hydrogen production from water. Adv. Funct. Mater. 20, 2255–2262.
Yeh, T.F., Cihlář, J., Chang, C.Y., Cheng, C., Teng, H., 2013. Roles of graphene oxide in photocatalytic water splitting. Mater. Today 16, 78–84.
Yu, S., Wang, Xiangxue, Pang, H., Zhang, R., Song, W., Fu, D., Hayatc, T., Wang, Xiangke, 2018. Boron nitride-based materials for the removal of pollutants from aqueous solutions: a review. Chem. Eng. J. 333, 343–360.
Yuan, Y.J., Chen, D.Q., Shi, X.F., Tu, J.R., Hu, B., Yang, L.X., Yu, Z.T., Zou, Z.G., 2017. Facile fabrication of "green" SnS_2 quantum dots/reduced graphene oxide composites with enhanced photocatalytic performance. Chem. Eng. J. 313, 1438–1446.
Zhang, F.M., Sheng, J.L., Yang, Z. Di, Sun, X.J., Tang, H.L., Lu, M., Dong, H., Shen, F.C., Liu, J., Lan, Y.Q., 2018. Rational design of MOF/COF hybrid materials for photocatalytic H_2 evolution in the presence of sacrificial electron donors. Angew. Chem. Int. Ed. 57, 12106–12110.

Zhang, L., Vasenko, A.S., Zhao, J., Prezhdo, O.V., 2019. Mono-elemental properties of 2D black phosphorus ensure extended charge carrier lifetimes under oxidation: time-domain ab initio analysis. J. Phys. Chem. Lett. 10, 1083–1091.
Zhang, N., Xu, Y.J., 2016. The endeavour to advance graphene-semiconductor composite-based photocatalysis. CrystEngComm 18, 24–37.
Zhang, N., Yang, M.Q., Liu, S., Sun, Y., Xu, Y.J., 2015. Waltzing with the versatile platform of graphene to synthesize composite photocatalysts. Chem. Rev. 115, 10307–10377.
Zhang, R., Wang, J., Han, P., 2015. Highly efficient photocatalysts of Pt/BN/CdS constructed by using the Pt as the electron acceptor and the BN as the holes transfer for H_2-production. J. Alloys Compd. 637, 483–488.
Zhang, X., Quan, X., Chen, S., Yu, H., 2011. Constructing graphene/$InNbO_4$ composite with excellent adsorptivity and charge separation performance for enhanced visible-light-driven photocatalytic ability. Appl. Catal. B Environ. 105, 237–242.
Zhang, Y., Liu, J., Wu, G., Chen, W., 2012. Porous graphitic carbon nitride synthesized via direct polymerization of urea for efficient sunlight-driven photocatalytic hydrogen production. Nanoscale 4, 5300–5303.
Zhang, Y., Tang, Z.-R., Fu, X., Xu, Y.-J., 2010. TiO_2-graphene nanocomposites for gas-phase photocatalytic degradation of volatile aromatic pollutant: is TiO_2-graphene truly different from other TiO_2-carbon composite materials? ACS Nano 4, 7303–7314.
Zhang, Y., Zhang, N., Tang, Z., Xu, Y., 2012. Graphene transforms wide band gap ZnS to a visible light photocatalyst. The new role of graphene as a macromolecular photosensitizer. ACS Nano 6, 9777–9789.
Zhang, Z., He, D., Liu, H., Ren, M., Zhang, Y., Qu, J., Lu, N., 2019. Synthesis of graphene/black phosphorus hybrid with highly stable P-C bond towards the enhancement of photocatalytic activity*. Environ. Pollut. 245, 950–956.
Zhao, H., Liu, H., Sun, R., Chen, Y., Li, X., 2018. A $Zn_{0.5}Cd_{0.5}S$ photocatalyst modified by 2d black phosphorus for efficient hydrogen evolution from water. ChemCatChem 10, 4395–4405.
Zhao, Y., Zhang, S., Shi, R., Waterhouse, G.I.N., Tang, J., Zhang, T., 2020. Two-dimensional photocatalyst design : a critical review of recent experimental and computational advances. Mater. Today 34, 78–91.
Zheng, D., Cao, X., Wang, X., 2016. Precise formation of a hollow carbon nitride structure with a janus surface to promote water splitting by photoredox catalysis. Angew. Chem. Int. Ed. 55, 11512–11516.
Zheng, Y., Jiao, Y., Zhu, Y., Li, L.H., Han, Y., Chen, Y., Du, A., Jaroniec, M., Qiao, S.Z., 2014. Hydrogen evolution by a metal-free electrocatalyst. Nat. Commun. 5, 1–8.
Zhi, Y., Li, Z., Feng, X., Xia, H., Zhang, Y., Shi, Z., Mu, Y., Liu, X., 2017. Covalent organic frameworks as metal-free heterogeneous photocatalysts for organic transformations. J. Mater. Chem. 5, 22933–22938.
Zhou, C., Lai, C., Huang, D., Zeng, G., Zhang, C., Cheng, M., Hu, L., Wan, J., Xiong, W., Wen, M., Wen, X., Qin, L., 2018a. Highly porous carbon nitride by supramolecular preassembly of monomers for photocatalytic removal of sulfamethazine under visible light driven. Appl. Catal. B Environ. 220, 202–210.
Zhou, C., Lai, C., Xu, P., Zeng, G., Huang, D., Li, Z., Zhang, C., Cheng, M., Hu, L., Wan, J., Chen, F., Xiong, W., Deng, R., 2018b. Rational design of carbon-doped carbon nitride/$Bi_{12}O_{17}Cl_2$ composites: a promising candidate photocatalyst for boosting visible-light-driven photocatalytic degradation of tetracycline. ACS Sustain. Chem. Eng. 6, 6941–6949.
Zhou, C., Lai, C., Zhang, C., Zeng, G., Huang, D., Cheng, M., Hu, L., Xiong, W., Chen, M., Wang, J., Yang, Y., Jiang, L., 2018c. Semiconductor/boron nitride composites: synthesis, properties, and photocatalysis applications. Appl. Catal. B Environ. 238, 6–18.
Zhou, J., Zhao, J., Liu, R., 2020. Defect engineering of zeolite imidazole framework derived ZnS nanosheets towards enhanced visible light driven photocatalytic hydrogen production. Appl. Catal. B Environ. 278, 119265.
Zhou, P., Zhang, Qinghua, Xu, Z., Shang, Q., Wang, L., Chao, Y., Li, Y., Chen, H., Lv, F., Zhang, Qing, Gu, L., Guo, S., 2020. Atomically dispersed Co–P3 on CdS nanorods with electron-rich feature boosts photocatalysis. Adv. Mater. 32, 1904249.
Zhu, M., Kim, S., Mao, L., Fujitsuka, M., Zhang, J., Wang, X., Majima, T., 2017a. Metal-free photocatalyst for H_2 evolution in visible to near-infrared region: black phosphorus/graphitic carbon nitride. J. Am. Chem. Soc. 2017 139, 13234–13242.
Zhu, M., Osakada, Y., Kim, S., Fujitsuka, M., Majima, T., 2017b. Black phosphorus : a promising two dimensional visible and near-infrared-activated photocatalyst for hydrogen evolution. Appl. Catal. B Environ. 217, 285–292.
Zhu, M., Sun, Z., Fujitsuka, M., Majima, T., 2018a. Z-scheme photocatalytic water splitting on a 2D heterostructure of black phosphorus/bismuth vanadate using visible light. Angew. Chem. Int. Ed. 57, 2160–2164.
Zhu, M., Zhai, C., Fujitsuka, M., Majima, T., 2018b. Noble metal-free near-infrared-driven photocatalyst for hydrogen production based on 2D hybrid of black phosphorus/WS_2. Appl. Catal. B Environ. 221, 645–651.
Zhu, X., Zhang, T., Sun, Z., Chen, H., Guan, J., Chen, X., Ji, H., Du, P., Yang, S., 2017. Black phosphorus revisited : a missing metal-free elemental photocatalyst for visible light hydrogen evolution. Adv. Mater. 29, 1605776.